UNIVERSITY OF CALGARY

Cavity-Enhanced Waveguide Quantum Memory

by

Hassan Mallahzadeh

A THESIS

SUBMITTED TO THE FACULTY OF GRADUATE STUDIES

IN PARTIAL FULFILLMENT OF THE REQUIREMENTS FOR THE

DEGREE OF MASTER OF SCIENCE

DEPARTMENT OF PHYSICS AND ASTRONOMY

CALGARY, ALBERTA

January, 2015

Abstract

An optical quantum memory is a device capable of storing the quantum state of a photon and subsequently recalling it faithfully. The efficiency of a memory, which is the focus of this work, is defined as the probability of successful storage and subsequent retrieval of the information. This thesis reports an experiment performed towards making a high efficiency quantum memory by using a cavity enhanced Atomic Frequency Comb (AFC) protocol, implemented in a waveguide in a rare-earth ion doped crystal. Our measurements identified the obstacles that have to be overcome to achieve that aim. Exploiting the cavity dynamics, we managed to estimate the essential parameters in implementation of the scheme. The investigations give a valuable insight into the protocol and the ways to exploit its full potential. Furthermore, the analysis of the experimental observations leads to proposals that may serve as alternatives to current ways of implementing the protocol.

Dedicated to the loving memory of my grandmother, who passed away a few days before I finished this thesis.

Table of Contents

List of Figures and Illustrations

Chapter 1

QUANTUM INFORMATION

From engraved religious commands in a tablet stone to the data that we store in internet clouds, there is no fundamental confusion between *dead* and *alive*, *do* and *don't* or *zero* and *one*. But this is not the case when we want to store the information in the context of one of the most profound discoveries of human kind, quantum mechanics. The quantum version of a binary system can be in a superposition of the states *dead* and *alive*, *do* and *don't* or *zero* and *one*. This fundamental property of quantum mechanics has opened a window to a new world of information and communication. It offers the possibility of making computers that are tremendously faster than their classical counterparts. An example is Shor's algorithm which is a quantum algorithm capable of factorizing a number into it's prime factors in an amount of time that increases linearly with the size of the number to be factorized [3]. In contrast, the classical algorithms require a time that grows exponentially with the size of the number. Needless to say, the proposed scheme can result in a huge enhancement of computational power.

Similar to a classical computer, a quantum computer needs some way of synchronizing the flow of information in order to process it. Synchronization in any kind of computer requires a medium to store information and retrieve it when needed. For the case of quantum information that medium is called a *quantum memory*.

Quantum memories have also important roles in communication of quantum information. Like classical bits, quantum bits (*qubits*) have to be transmitted between distant parties. Photons are a natural choice for this task since qubits can be encoded in their various degrees of freedom and they can be sent through optical fibers and processed by simple optical components. However, undesired interaction of photons with the surrounding medium adds

serious complications to transmission of photons between distant parties. For example a 1.5 μm photon transmitted through a telecommunication fiber will be lost with a probability of 50% after 15 km and this probability converges exponentially to one as the length of the fiber increases [4]. This loss can't be overcome by merely using optical amplifiers, such as those used in classical optics, since the no-cloning theorem forbids the creation of identical copies of an unknown quantum state and hence amplification without adding noise [5].

The quantum repeater has been proposed to solve this issue. As we will explain in the following section, quantum memory capable of mapping information encoded into a photon to a storage medium and then retrieve the information by sending out another photon is a necessary ingredient of the quantum repeater scheme. Because it stores photons, the aforementioned quantum memory is called an *optical quantum memory*. This is the subject of this thesis.

1.1 Entanglement distribution

1.1.1 Quantum Entanglement

An entangled quantum state is in simple words a state that can not be decomposed into a simple product of it's individual subsystems [3]. For example, if the state of two particles A and B is denoted by $|\psi\rangle_{AB}$ then

$$|\psi\rangle_{AB} \neq |\psi\rangle_A |\psi\rangle_B \tag{1.1}$$

implies that the particles are entangled. A state of two qubits is regarded as *maximally* entangled if measuring each of them along *any* axis on the Bloch sphere (a convenient and often used way to depict states or projective measurements) results in a completely random result[3]. In other words such a measurement won't provide any information about the individual qubits. For instance consider the following state

$$|\phi^+\rangle_{AB} = \frac{1}{\sqrt{2}} \left(|00\rangle_{AB} + |11\rangle_{AB}\right) \ . \tag{1.2}$$

The *density matrix* of the above is represented by

$$\rho_{AB} = |\phi^+\rangle\langle\phi^+| = \frac{1}{2}\begin{pmatrix} |00\rangle\langle 00| & |00\rangle\langle 11| \\ |11\rangle\langle 00| & |11\rangle\langle 11| \end{pmatrix} , \tag{1.3}$$

and the density matrix of the first qubit is given by tracing over the second qubit

$$\rho_A = tr_B\left(|\phi^+\rangle\langle\phi^+|\right) = \frac{1}{2}I_A , \tag{1.4}$$

in which tr_B is the *partial trace* over subsystem B and is defined as

$$tr_B M_{AB} = \sum_i \langle i|_B M_{AB} |i\rangle_B , \tag{1.5}$$

and $|i\rangle_B$ is the basis of system B. It can be seen from equation 1.4 that measuring qubit A along any axis results in a completely random outcome.

$|\phi^+\rangle$ is one of four maximally entangled states that form a basis for any two qubit system. These mutually orthogonal states are

$$|\phi^\pm\rangle = \frac{1}{\sqrt{2}}\left(|00\rangle_{AB} \pm |11\rangle_{AB}\right), \quad |\psi^\pm\rangle = \frac{1}{\sqrt{2}}\left(|01\rangle_{AB} \pm |10\rangle_{AB}\right) . \tag{1.6}$$

The above states are known as *Bell-states* and play a central role in many applications of quantum communication. In the following subsection we will explain the role of Bell-states in distributing entanglement between two distant parties.

1.1.2 Quantum Repeaters

When some entangled pairs are available, the *entanglement swapping* technique can be used to establish entanglement over larger distances by quantum mechanically "tying" the entangled pairs' ends together.

The entanglement swapping idea is that if one party has a pair of maximally entangled particles A, B and another party has another pair of maximally entangled particles C, D (as in figure 1.1) one can see mathematically that the combined state of the parties can be

written as a combination of maximally entangled pairs between A, D and B, C. For example

$$|\phi^+\rangle_{AB}|\phi^+\rangle_{CD} = \frac{1}{2}\left(|\phi^+\rangle_{AD}|\phi^+\rangle_{BC} + |\phi^-\rangle_{AD}|\phi^-\rangle_{BC} + |\psi^+\rangle_{AD}|\psi^+\rangle_{BC} + |\psi^-\rangle_{AD}|\psi^-\rangle_{BC}\right) . \tag{1.7}$$

Thus projecting the pair of particles B, C onto one of the Bell states, by means of a so called *Bell State Measurement* (BSM), results in having the particles A, D in one of the Bell states and so entanglement is established between A, D [6].

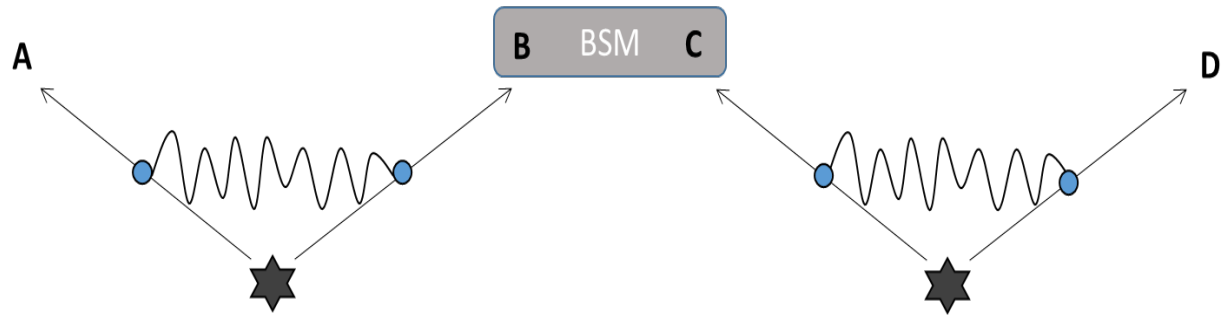

Figure 1.1: Entanglement Swapping; Performing a Bell State Measurement on the two central photons establishes entanglement between distant right and left photons.

Photon pair creation is probabilistic by nature and as mentioned before, photons can be lost during transmission through optical fibers, which is also a stochastic process. In addition, depending on the used scheme, the BSM has a limited probability of success. As a result, entanglement swapping only succeeds probabilistically and it is not predictable when one has an entangled pair between the two points A, D.

Now if one has two such *elementary links* (which may have succeeded in establishing entanglement), like in picture 1.2, and want to perform another BSM on the photons A_2, D_1 to swap the entanglement to photons A_1, D_2, the synchronization issue arises. BSM has to be done on a pair of identical photons at a particular instant of time [7], so the BSM measurement at the node requires synchronization of the photons that it receives. Assuming photon pair creation sources that are capable of sending out multiple pairs each at a different mode

(e.g. frequency modes) increases the probability of success. However the BSM station at the node has to know which photons that it has received are part of an already entanglement swapped pair. Therefore, the BSM stations at the links must be able to send the measurement results to the BSM at the node by classical signals, so that the node station can filter out the photons that are not part of an already entanglement swapped pair. Consequently, the BSM station at the node has to be able to store the photons that it receives long enough to classically receive the result of the BSM at the links.

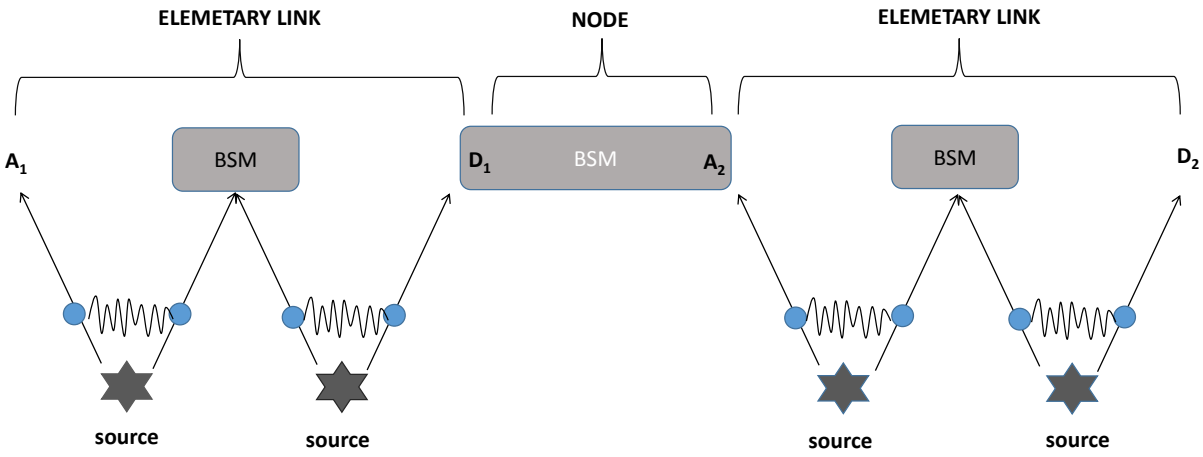

Figure 1.2: Extending entanglement by performing a BSM at the central node to entangle photons A_1 and D_2 needs synchronization of photons D_1 and A_2.

Here the optical quantum memories come to the picture, which store the photons that are required to be synchronized (D_1, A_2). As stated before, the memories must be able to store the photons during a time that is required for the classical signals to reach the BSM station at the node. One can now add more and more nodes and elementary links to keep extending the entanglement over larger distances. The above *quantum repeater* scheme can increase the success rate of entanglement distribution [5].

Assume that the probability of successful arrival of a photon to a particular point is

given by $10^{-\alpha l}$ in which l is the distance that has to be traveled and ρ is the probability of a successful entangled pair generation at a source. η_m represents the efficiency of an optical quantum memory, which is defined as the probability of successful storage and retrieval of a photon. The number of modes, which is basically the number of photons that can be stored simultaneously and distinguishably in a quantum memory, is denoted as m. The number of links, the total channel length and the probability of a successful BSM are represented by n, L and p_b. It is shown in the supplementary information of reference [7] that the success rate of entanglement distribution is be given by

$$\frac{cn}{L} p_b^{n-1} \left(\eta_m \eta_d\right)^{2n} \left(1 - \left(1 - p_b \rho^2 \eta_d^2 \left(10^{-\alpha \frac{L}{n}}\right)\right)^m\right)^n \ , \tag{1.8}$$

in which c is the speed of light. In driving equation 1.8, it is assumed that the distant parties themselves have a quantum memory each so that they can hold their photons and filter out those which are not a part of an entangled pair.

To quantitatively show the advantage of using a quantum repeater scheme we assume $\rho = \eta_m = \eta_d = 0.9$, $p_b = 0.5$ (the maximum BSM efficiency using linear optics), $m = 1000$ (a reasonable number for a quantum memory implemented in rare earth ion doped crystals, see chapter 3) and $\alpha = 0.2\ dB/km$ (the typical loss in a regular telecommunication fiber). Figure 1.3 shows how the success rate changes when one uses a quantum repeater scheme with five or nine elementary links and also when the quantum repeater scheme is not used. More comprehensive versions of the figure are given in [7].

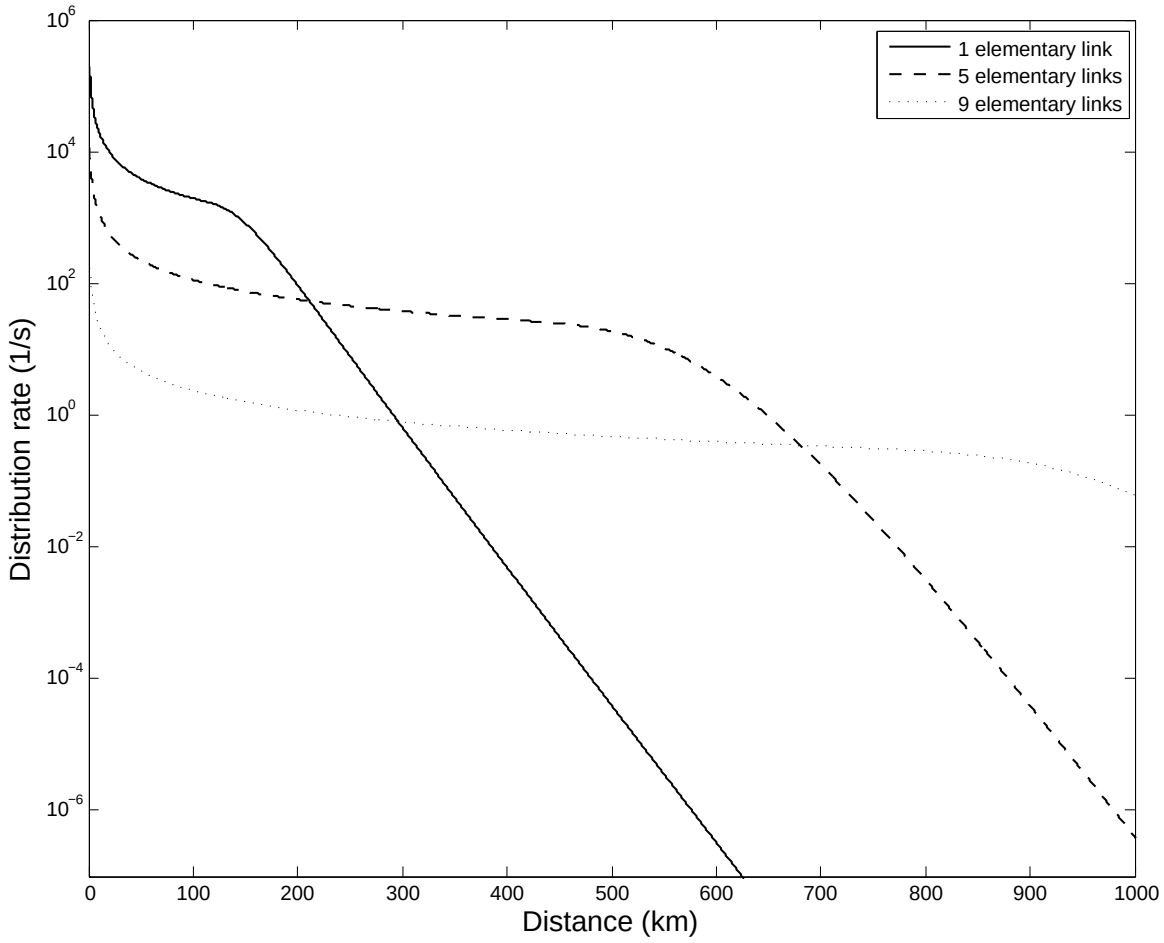

Figure 1.3: Entanglement distribution rate for quantum repeater scheme with a) nine elementary links (dotted line) , b) five elementary links (dashed line), and c) one elementary link (no quantum repeater, solid line).

A look at equation 1.8 reveals the importance of having efficient quantum memories, especially when the number of elementary links is large. The distribution rate quickly drops to zero when the efficiency of quantum memories is reduced, so one has to use the most efficient memories. A good example might be the simple case in which just five elementary links are used. If you consider a quantum memory that is twenty percent efficient, the success rate is three orders of magnitude larger than when using a ten percent efficient quantum memory. Needless to say, more efficient quantum memories can save a considerable amount of time and resources when implementing a quantum repeater scheme.

1.2 Performance criteria for quantum memories

In addition to high efficiency, a good quantum memory must fulfill the following requirements [4]. First, the state of the retrieved photon must be close to state of the stored photon. This similarity is quantified by the *fidelity* [3]. Second, the storage time has to be long enough for the particular task. Third, the number of optical modes that a quantum memory can store should be sufficiently high for the task to be performed. Having a large acceptance bandwidth, being robust, simple to operate and compatible with other optical components are also required for a *good* quantum memory. In this thesis however the focus is on efficiency of the quantum memory.

Chapter 2

THE ATOMIC FREQUENCY COMB QUANTUM MEMORY PROTOCOL

The *Atomic Frequency Comb* (AFC) protocol was proposed as a scheme for quantum memories and was inspired by the idea of periodical spectral hole burning in an absorptive medium for frequency domain data storage and time domain retrieval of a pulse [8][9]. This protocol has been successfully implemented in independent experiments (see e.g. [1]). In this chapter we will cover the mathematical and physical concepts that make an AFC a functional quantum memory scheme.

2.1 The Atomic Frequency Comb, the frequency filter picture

Even though the AFC memory is used for quantum state storage, it can be fully understood by using the relatively simple classical picture of a periodic frequency filter.

The main idea probably stems from the concept of the *Dirac Comb* or *Shah* function, which is an infinite series of evenly and periodically spaced delta Dirac functions. In the frequency domain it is represented as

$$S(\nu) = \sum_{i=-\infty}^{i=+\infty} \delta\left(\nu - i\Delta_\nu\right) \ . \tag{2.1}$$

Performing a Fourier transform to the time domain gives [10]

$$\tilde{S}(t) = \frac{1}{\Delta_\nu} \sum_{i=-\infty}^{i=+\infty} \delta\left(t - \frac{i}{\Delta_\nu}\right) \ , \tag{2.2}$$

which is another infinite series of delta functions and the interval between two successive delta functions is the reciprocal of the interval in the frequency domain.

The multiplication of a Shah function in the frequency domain with an arbitrary function that is much wider than Δ_ν provides a uniform frequency *sample* of the arbitrary function

which from now on we assume is a pulse in the frequency domain. The Fourier transform of the frequency sample to the time domain is given by

$$\mathscr{F}\left(S(\nu)P(\nu)\right) = \int_{-\infty}^{\infty} \tilde{S}(t)\tilde{P}(t-\tau)\mathrm{d}\tau \ , \tag{2.3}$$

which, as shown in figure 2.1, results in having an infinite number of pulses in the time domain at places of the delta functions. This leads to the idea of using a frequency filter to deliver identical output pulses (or *echoes*) from the input pulse. However, this mathematical scheme opposes two fundamental rules of physics. First of all, it is against causality. Echoes can not exist before the interaction of the original pulse with the frequency sampler. Second, having an infinite number of identical pulses is to have a system with infinite energy. The conservation of energy rule requires the output pulses after interaction with the frequency sampler to have an energy at most equal to the input pulse's energy. The last statement comes from regarding the frequency sampler as a *passive* filter that can not add energy to the output.

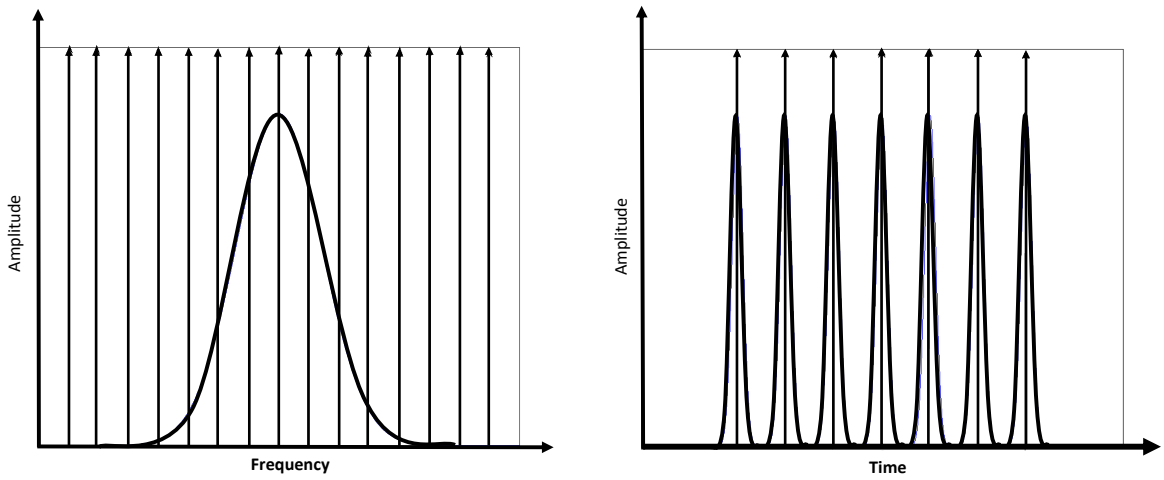

Figure 2.1: Multiplication of a Shah function and a pulse (left), and the Fourier transformation in the time domain (right). Peaks are delta functions.

A physical frequency sampler (filter) follows casualty thanks to the fact that each absorption spectrum has to be accompanied by a dispersion spectrum [11] [1]. Furthermore, for a causal system, the mere fact that real delta Dirac absorption lines can not be made in a non-abstract world imposes the energy conservation restriction. This is because the finite linewidth of absorption peaks in the frequency domain translates to echoes in the time domain that converge to zero over time [2].

Derivation of the dispensation spectrum from any absorption spectrum constitutes solving the Kramers-Kronig relations. Although these relations are often taught as the connection between real and imaginary parts of the electric susceptibility, they hold for *any* background-subtracted frequency space response function that represents a physical system [11] [3].

For a medium that has a complex refractive index, the interaction of an electrical field with the medium results in an output field of the form

$$E_o(\omega, x) = e^{i\tilde{k}(\omega,x)} E_i(\omega) \ , \tag{2.4}$$

in which E_i and E_o represent input and output electric fields, x is an arbitrary point inside the medium, ω is the angular frequency and $\tilde{k}$ is the complex wavenumber [4]. Taking the derivitive of the above with respect to x gives

$$\frac{dE_o(\omega, x)}{dx} = i\tilde{k}(\omega, x) E_o(\omega, x) \ . \tag{2.5}$$

In the above $\tilde{k}$ can be regarded as a response function and so it has to follow the Kramers-Kronig relations. The absorption spectrum of a sample, which is the imaginary part of $\tilde{k}$, is what can be directly calculated by knowing the intensity of the input and output fields.

[1] Actually, the dispersion spectrum emerges from the causality axiom, but we are free to think in reverse.

[2] The dispersion spectrum and shape of the peaks can result in oscillations in the pattern of the echoes, but they generally approach zero over time

[3] The response function is a function that is multiplied with an input to produce an output (response). The background, when the equations are written for the electric susceptibility is zero and for the electric permittivity is the vacuum permittivity ϵ_0.

[4] The complex wave number is defined as $\tilde{k} = \frac{\tilde{n}\omega}{c}$ in which $\tilde{n}$, ω and c are the complex index of refraction, the angular frequency, and the speed of light in vacuum, respectively.

When the absorption spectrum is known, the dispersion spectrum can be derived using the Kramers-Kronig relations to derive the real part of $\tilde{k}$.

2.2 Atomic Frequency Comb memory, the atomic implementation

Although optical cavities are the best known frequency filters, it is not easy to change their round trip time (which can be seen as the "storage" time) and they offer limited flexibility in terms of optimizing the shape of the absorption peaks. In order to change the round trip time of a Fabry-Pérot cavity, either it's length or the index of refraction of the medium between the mirrors has to change. The latter can hardly be changed considerably for most mediums and the former has negative consequences, such as increasing complexity and introduction of additional loss. In addition, it is mathematically proven that the maximum memory efficiency is given by a square shaped frequency filter [12], which can not be formed by an optical cavity [5]. Moreover, even though modifying the effective mirror reflectivities might be possible [6], it can result in instabilities and additional unwanted loss. For these and other reasons, cavities are not practical to be used as frequency filter memories. Luckily, there exists options other than cavities for making a frequency filter.

Each chemical element has it's own specific absorption spectrum and a proper atomic medium can be engineered to make high quality and flexible filters. In the following subsections, we briefly review the properties of the rare-earh ion doped crystals that make them a practical choice for making an *Atomic* Frequency Comb.

2.2.1 Line-width broadening

In nature an infinitely sharp absorption peak can not be created. The existence of infinitely sharp absorption peaks, would result in the violation of energy conservation, as mentioned in the previous section. For an atomic medium, in general there exist two main absorp-

[5] For example a cavity formed by flat mirrors can just form absorption peaks with Airy function shape[11].
[6] One way is to replace simple mirrors by judiciously chosen additional cavities (see chapter 5)

tion linewidth broadening mechanisms which are called *homogeneous* and *inhomogeneous* broadening. For an isolated atom, *homogeneous* linewidth broadening happens due to finite lifetime of any excited state [13, 14]. The finite lifetime in the time domain translates to a broadened absorption line in the frequency domain. This can be understood by the quantum energy-time uncertainty relation or from the classical Fourier transformations [14]. When an atom is placed inside an atomic medium, interactions with the medium may result in further broadening of the homogeneous linewidth [13]. In any case, the homogeneous linewidth gives the maximum theoretical frequency resolution that an absorption spectrum can be engineered to.

Inhomogeneous linewidth broadening appears when the host medium surrounding the absorptive atoms is not uniform. Surface effects, impurities, imperfections and non-even distribution of atoms and ions are among the causes that result in inhomogeneous broadening.

Inhomogeneous broadening causes individual atoms to have slightly different absorption spectra and consequently the combined spectrum of an ensemble of atoms may have an absorption linewidth much larger than the homogeneous linewidth [13]. This concept is illustrated in figure 2.2.

It is imaginable that tailoring the inhomogeneous linewidth in a suitable material can generate the frequency filter required for the AFC protocol. A suitable material must have a wide inhomogeneous linewidth and a narrow homogeneous linewidth. The former condition makes a wide range of frequencies available for storing the information and the latter guarantees (in principle) a high resolution in the frequency domain. Such a medium can store a large number of pulses, which, at the single photon level [7], translates to a high multimode storage capacity. In addition it can have a large storage time, since the absorption peaks in the frequency domain can be very close to each other.

[7] In the AFC theory, a single photon's probability distribution in the frequency domain corresponds to a classical pulse with finite width in the frequency domain. In this thesis the word "pulse" is interchangeable with photon's probability distribution, either in the time domain or the frequency domain.

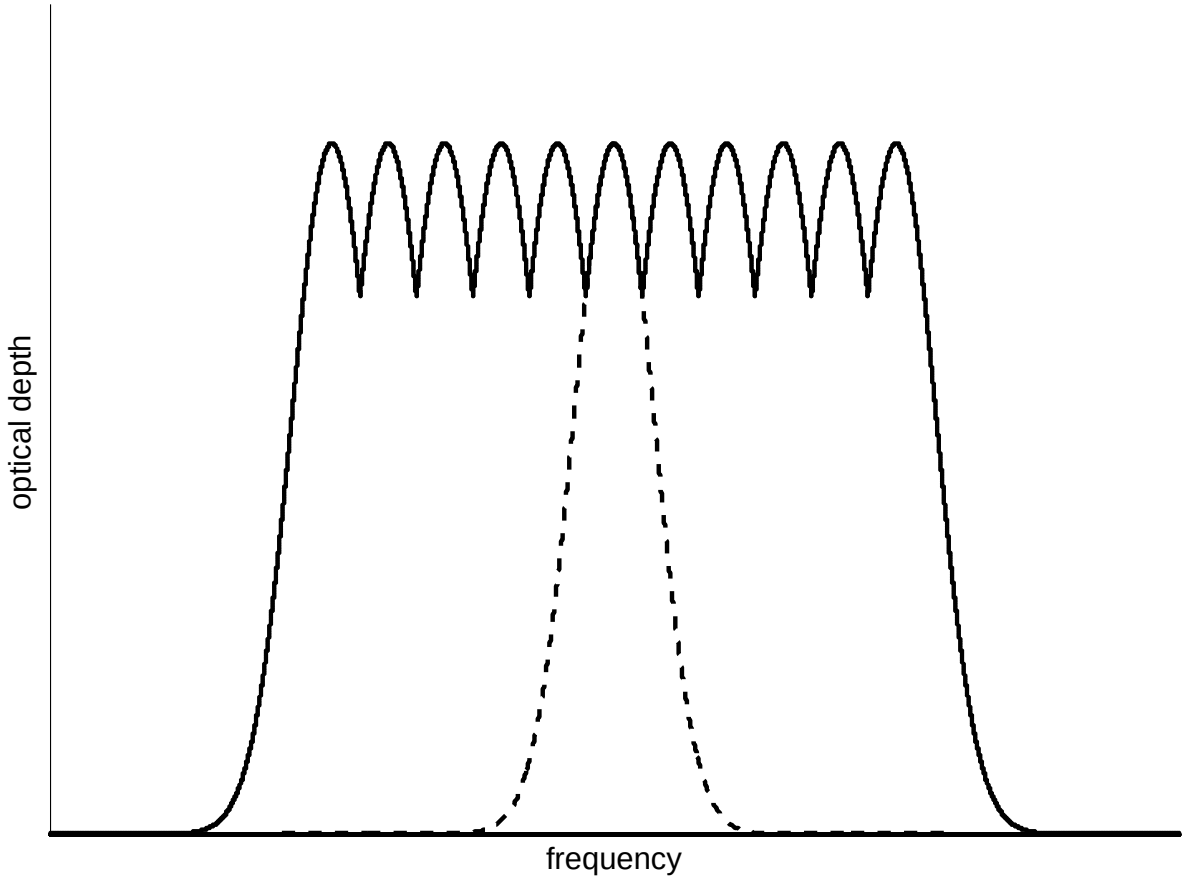

Figure 2.2: Homogeneous and inhomogeneous linewidths. The inhomogeneous linewidth (solid line) is an accumulation of homogeneous linewidths (broken line).

2.2.2 Rare-earth ion doped crystals as a host for the AFC

The rare-earth (RE) metals are predominately the lanthanide group of elements with atomic numbers from 58 (lanthanum) to 71 (lutetium) [8]. At cryogenic temperatures, RE compounds generally have very sharp absorption spectra even in comparison with single atoms of other elements [14]. The sharp absorption peaks (narrow homogeneous linewidth) can be justified by investigating their electronic configuration. Eleven out of fifteen lanthanides have electronic configuration of the form $[Xe]\,4f^n6s^2$ where n runs from three to fourteen but does not

[8]The International Union of Pure and Applied Chemistry (IUPAC), defines RE metals as lanthanides plus scandium and yttrium with atomic numbers 21 and 39 respectively [15]. In this work we follow the tradition of quantum memory researchers according to which, lanthanides and RE elements are interchangeable words.

include eight. The remaining four elements have electronic configuration of $[Xe]\,4f^n5d^16s^2$ where n is 0, 1, 7 or 14 [16]. Lanthanides normally form trivalent ions -denoted by RE^{3+}- in chemical compounds [9] and the electronic configuration of the former category of atoms gets altered to $[Xe]\,4f^{n-1}$ and the latter category to $[Xe]\,4f^n$ where n is the number of electrons in the $4f$ orbital for the corresponding neutral atoms [17]. The electronic configuration of $[Xe]$ (Xenon), which is a stable noble gas, contains two electrons in orbital $5s$ and six electrons in orbital $5p$. The principal number of these electrons is larger than the $4f$ electrons in (RE^{3+}) ions, which indicates that the $4f$ electrons fall *inside* the stable shell of the Xenon configuration. $5s$ and $5p$ electrons provide an effective shell that protects the $4f$ orbital from perturbations from the surrounding medium, which consequently result in a narrow homogeneous linewidth. In spite of this, the interactions with the medium is large enough to allow the existence of a large inhomogeneous linewidth [13].

Rare-earth ions experience some broadening of their homogeneous linewidth primarily due to thermally excited phonons in the host lattice. In order to suppress the phonons, the sample has to be cooled down to cryogenic temperatures [14]. The reduced phonon density at low temperatures also leads to longer level lifetimes, which consequently makes the AFC structure long lasting.

Thulium is the RE element used in this work. It's trivalent configuration is $[Xe]\,4f^{12}$ and is denoted by the chemical symbol Tm^{3+}. The host material is lithium niobate, which is a transparent compound of niobium, lithium, and oxygen with chemical representation $LiNbO_3$.

The energy sub-levels of the $4f$ orbital are represented in L-S notation as ${}^{2S+1}L_J$, where S is the total spin number, J is the total angular momentum quantum number and L represents the total *orbital* angular momentum quantum number. In the absence of a magnetic field the relevant levels in this representation are ${}^3H_6$ as the ground state,${}^3H_4$ as the excited state and ${}^3F_4$ as a bottleneck state with an energy level between the ${}^3H_6$ and ${}^3H_4$ levels [13].

[9] The only exceptions in nature are Cerium $\left(Ce^{4+}\right)$ and Europium $\left(Eu^{2+}\right)$.

Exciting the atoms from the ground state sends the electrons to the excited state, which has a (radiative) lifetime of 82 μs. When atoms start spontaneously decaying from the excited state about 56% of them go back to the ground state but 44% will go to the bottleneck state, which at $4K$, has a lifetime of 2.4 ms [1]. If one continues to excite the atoms in a specific frequency interval during a time that is shorter than the life time of the $^3F_4$ level, in principle one can remove atoms from the ground state and create a *transmission window* with low atomic absorption in the frequency interval. However, 2.4 ms is not enough time to avoid the effect of spontaneous emission from the excited state, which would *contaminate* the signal of any stored photons [4].

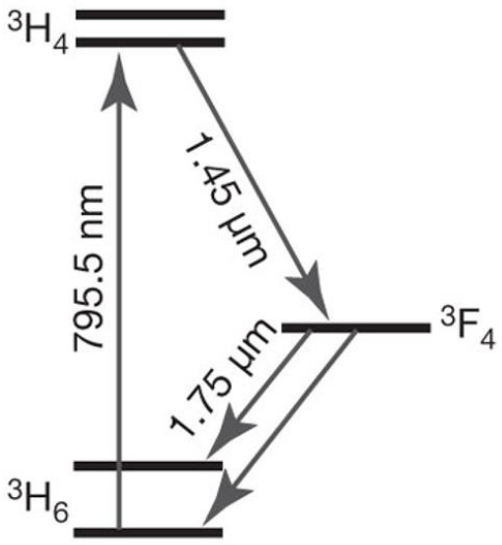

Figure 2.3: Simplified energy level diagram of thulium ions. Upon application of a magnetic field of 570G, the ground and excited levels split into magnetic sublevels with the ground state lifetime exceeding one second at $4K$. This figure is taken from [1].

To solve this problem, a constant magnetic field has to be applied to the crystal. A magnetic field of 570 Gauss splits the ground and excited state each into two sublevels with the ground state lifetime exceeding one second at $4K$ (see figure 2.3) [1]. These sublevels are formed due to the fact that the magnetic field removes the degeneracy of the nuclear

Zeeman levels in the $^3H_6$ and $^3H_4$ states. These states may be denoted as $|e\rangle_+$ and $|e\rangle_-$ for the sublevels of $^3H_6$ (the excited state) and $|g\rangle_+$ and $|g\rangle_-$ for the sublevels of $^3H_4$ (the ground state). Consequently, a single laser frequency applied to the inhomogenious linewidth will be in resonance with four classes of transitions: $|g\rangle_+ \rightarrow |e\rangle_+$, $|g\rangle_+ \rightarrow |e\rangle_-$, $|g\rangle_- \rightarrow |e\rangle_+$ and $|g\rangle_- \rightarrow |e\rangle_-$ [18]. As stated above, a portion of the excited atoms decay to the bottleneck ($^3F_4$) state. When these atoms leave the bottleneck state, they may decay to the upper or lower ground states. Repeating this procedure gives rise to three *holes* and six *anti-holes* in the absorption spectrum, as depicted in figure 2.4.

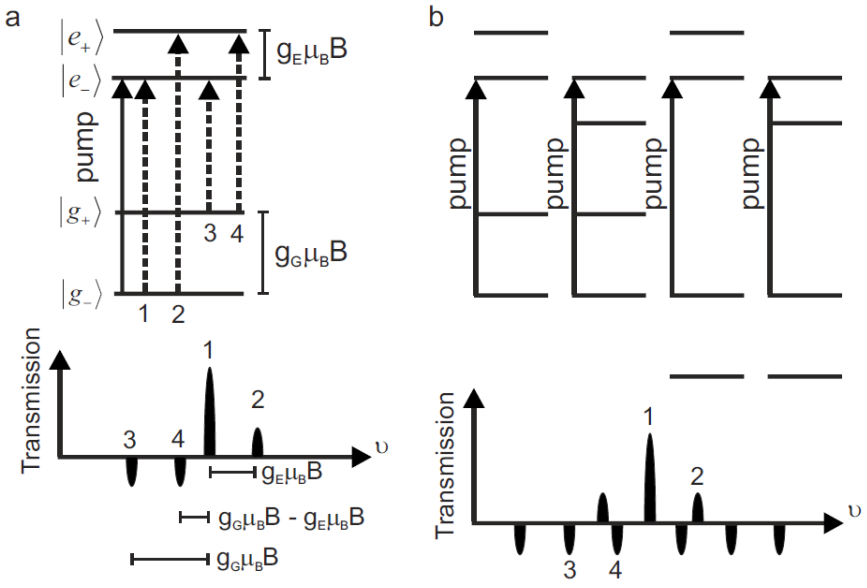

Figure 2.4: (a) Four-level hole burning spectrum (Zeeman levels) for the class of ions where the laser is in resonance with the $|g\rangle_- \rightarrow |e\rangle_-$ transition. The g_G (g_E) are the g factor for the ground (excited) state, μ_B is the Bohr magneton, and B is the applied magnetic field. The pump transition (solid line) and possible probe transitions(dashed lines) between the four levels are shown in the energy diagram and labeled on the corresponding transmission spectrum of holes and anti-holes. (b) Four level hole burning spectrum with inhomogeneous broadening. The four different classes of ions within the inhomogeneous profile that are in resonance with the pump beam are shown, along with the resulting transmission spectrum of holes and anti-holes. The figure and caption are taken from reference [2]

Nevertheless, the probability of nuclear spin-flip in thulium ions that are doped into

lithium niobate, by mere optical excitation is low, and therefore, only the transitions $|g\rangle_- \rightarrow |e\rangle_-$ and $|g\rangle_+ \rightarrow |e\rangle_+$ tend to be excited by light [19]. Consequently just two classes of transitions are possible and they can result in just one hole (indicated by the number 1 in figure 2.4) and a pair of anti-holes (indicated by the number 4 in figure 2.4).

Repeating the above procedure at equal frequency intervals can create an AFC. However, the existence of the anti-holes gives rise to complications that have to be taken into account before starting the AFC burning procedure. The interval between a hole and its corresponding anti-holes is basically determined by the magnetic field strength, as is realized from the caption of figure 2.4. If this interval is equal to the value that corresponds to a desired storage time, the anti-holes will fill out the holes and in the worst case there will remain no trace of an AFC [18].

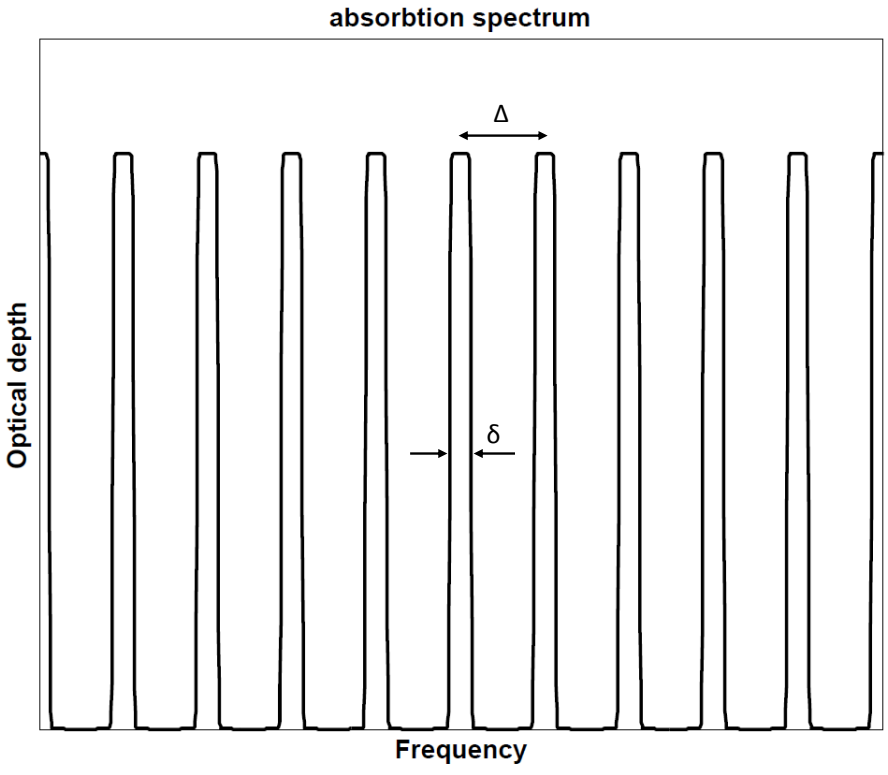

Figure 2.5: AFC linewidth (δ) and AFC pick separation (Δ).

The AFC finesse is defined as $F = \frac{\Delta}{\delta}$ where F denotes the finesse, δ is the peak width and Δ is the peak separation (peak to peak interval), as depicted in figure 2.5. An AFC with a finesse equal to two can be tailored in the absorption spectrum by setting the interval between a hole and its corresponding antiholes equal to half of the interval required for the desired storage time. This is depicted in figure 2.6. If one intends to make an AFC with a finesse larger than two, the magnetic filed must be strong enough to place the anti-holes outside of the frequency span of the AFC.

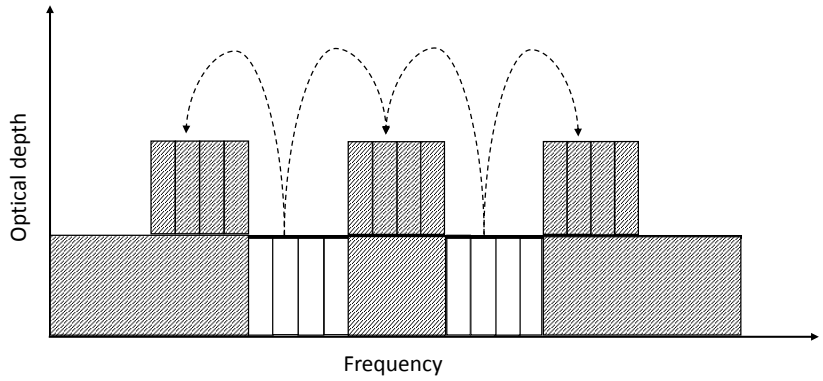

Figure 2.6: The procedure of making an AFC with finesse 2. the "slabs" that are removed from the absorption spectrum are placed at the corresponding slots on the adjacent intervals, which are as wide as the "trenches" that are to be carved. A similar strategy can be used to make an AFC with finesse 3/2.

The AFC made in the above described fashion is also known as a *persistent* AFC and the corresponding echoes are dubbed persistent echoes, because the filter has a long life time. A persistent AFC does not add any energy to the probe photons (photons that are to be stored), which is a crucial feature for the AFC memory to be considered a quantum memory. The filter pattern may be tailored in the excited state (since atoms in the excited state are removed from their conventional place in thermal equilibrium) during the excited state's lifetime. However, this filter can not be regarded as a quantum memory since the spontaneous emission adds noise to the echoes. Because this filter has a short life time it is

called a *transient* AFC and the corresponding echoes are dubbed transient echoes. Unless otherwise stated, in this work by "AFC" we mean "persistent AFC".

2.3 The Atomic Frequency Comb, the quantum memory picture

The implementation of a frequency comb quantum memory in an atomic medium suggests that the proper analysis of the system's response ought to be done in a quantum picture and that the classical treatment such as a frequency filter picture might not be suitable. However, as pointed out in reference [20], negligible population in the excited state implies validity of an approximate linearized Maxwell-Bloch model and consequently equivalence between classical and single photon dynamics. However for the sake of completeness we provide the quantum model that describes how an AFC can serve as a quantum memory for single photons.

The photon has a probability distribution in the frequency domain and after absorption by the ensemble it is stored in the collective atomic state described by [8]

$$|\psi\rangle = \sum_{j=1}^{N} c_j e^{i\delta_j t} e^{-ikz_j} |g_1 ... e_j ... g_N\rangle, \tag{2.6}$$

where z_j is the position of the atom j, k is the (central) wave number of the photon's wave packet, δ_j the detuning of the atom with respect to the (central) frequency of the photon and c_j denotes an amplitude that depends on the particular atom j. At $t = 0$ all atoms are in phase, but the state dephases as time passes since the δ_j's are different. In order to get a high probability of collective re-emission, the atomic detunings have to be engineered so that after some time the state rephases. If an AFC structure with sharp peaks is considered, one can write $\delta_j = m_j\Delta$ where m_j are integers and Δ is the comb peak separation in the frequency domain. It can be seen that in this case the initial state is reestablished after times $\frac{n}{\Delta}$ where n is a non-negative integer. At these times collective emission is triggered and echoes are emitted.

2.4 Efficiency of the AFC protocol

2.4.1 Analytic Calculation

The efficiency of an AFC quantum memory is often defined as the power of the first echo divided by the power of the input pulse, and we use this definition in this thesis. Calculating the efficiency of the AFC protocol can be easily done by assuming that the pulse (or photon's probability distribution) in the frequency domain is much wider than the peak to peak interval of the comb in the frequency domain and much narrower than the whole AFC bandwidth. In mathematical terms $\Delta \ll \gamma_p \ll \Gamma$, where Δ is the peak separation (peak to peak interval), γ_p is the photon bandwidth and Γ is the AFC bandwidth. In addition, it is assumed that the pulse width in the time domain, τ, is much wider than the time required for the pulse to pass the length of the storage medium. This assumption leads us to rule out all retardation effects caused by the difference in index of refraction of the medium and vacuum. In this case the average optical depth of the AFC is given by $\tilde{d} = \frac{d}{F}$ [10] where d is the optical depth of an AFC peak and F is finesse of the AFC.

What has to be calculated is the probability amplitude that a photon that reaches a specific point inside the crystal, gets absorbed, is reemitted there and subsequently reaches the end of crystal. Finally, an integral has to be taken over the whole length of the crystal. It can be represented by

$$\int_0^L dz' e^{-\tilde{\alpha}z'/2}\sqrt{\tilde{\alpha}}\sqrt{\tilde{\alpha}}e^{-\tilde{\alpha}(L-z')/2} = \tilde{\alpha}Le^{-\tilde{\alpha}L/2} \ . \tag{2.7}$$

In the above L is the length of the crystal, z' is an arbitrary point inside the crystal and $\tilde{\alpha} = \tilde{d}/L$. In the left side of equation 2.7 the first term gives the probability amplitude that the photon reaches the point z'. The second term is the probability amplitude that the

[10] This is obvious when the AFC has square shape peaks. For an AFC with Gaussian shape peaks $\tilde{d} = \frac{d}{F}\sqrt{\frac{\pi}{4\ln 2}} \approx \frac{d}{F}$ [8].

photon gets absorbed there [11]. The third term is the probability amplitude that the photon is reemitted and lastly the fourth term is the probability amplitude that the photon reaches the end of the crystal without being absorbed on the way. In writing the above formula, it is considered that the probability of absorbing a photon is equal to the reemission probability due to time reversal symmetry [21].

One factor has to be added to the calculation of the efficiency and that is the dephasing due to the finite width of the peaks. This dephasing can be understood by considering the frequency filter picture. In this picture the narrowest feature in the frequency domain is the peak width and in the time domain it will be the widest feature that covers the whole response in the time domain. It is clear that generally sharper peaks in the frequency domain result in slower dephasing in time domain. In addition, the efficiency is defined in regard to intensities not amplitudes. Therefore the efficieny is

$$\mu = (\tilde{\alpha}L)^2 \, e^{-\tilde{\alpha}L} \mu_{deph} = \tilde{d}^2 e^{-\tilde{d}} \mu_{deph} \ , \tag{2.8}$$

where μ_{deph} is the dephasing factor with regard to intensities. From this equation one can see that for constant finesse, the efficiency is maximum when $\tilde{d}$ is equal to 2 and can be at most 54% [12].

2.4.2 Computational Results

The efficiency of the AFC protocol in a more general case i.e. when the condition $\Delta \ll \gamma_p \ll \Gamma$ does not hold or when the AFC structure is not uniform can be quite cumbersome to calculate analytically. Fortunately a computer can be programmed to perform the computational task and provide the results numerically. Solving Maxwell-Bloch equations numerically is a method used in a lot of literature e.g. [22]. In this project we used the

[11] $\sqrt{\tilde{\alpha}}$ represents the absorption probability amplitude because the intensity follows the relation $I(z+dz) = e^{-\tilde{\alpha}dz} I(z)$ and so $I(z+dz) - I(z) = -\tilde{\alpha} I(z) dz$. Therefore the probability of absorption at the element of space is $\tilde{\alpha}dz$ and the corresponding probability amplitude is $\sqrt{\tilde{\alpha}}dz$.

[12] μ_{deph} is a function of finesse and peak shape and is independent of optical depth. The 54% limit is due to the first two terms of equation 2.8.

frequency filter picture, with the assumption of long decay time for the AFC structure in comparison to the storage time and also in comparison to decoherence due to finite peak linewidth. Towards this end we wrote a MATLAB code (appendix A) that has the pulse in the time domain and the absorption spectrum in the frequency domain as inputs. After deriving the dispersion spectrum from the Kramers-Kronig relations described in section 2.1, the total response function of the medium is at hand. Then it is multiplied by the pulse in the frequency domain, and a subsequent Fourier transform to the time domain delivers the output pulses. Figure 2.7 compares the theoretical result of efficiency as a function of optical depth from equation 2.8 with three numerically computed cases: 1) $\Delta \ll \gamma_p \ll \Gamma$ holds, 2) $\Delta \ll \gamma_p$ holds but $\gamma_p \ll \Gamma$ does not hold, 3) $\gamma_p \ll \Gamma$ holds but $\Delta \ll \gamma_p$ does not hold.

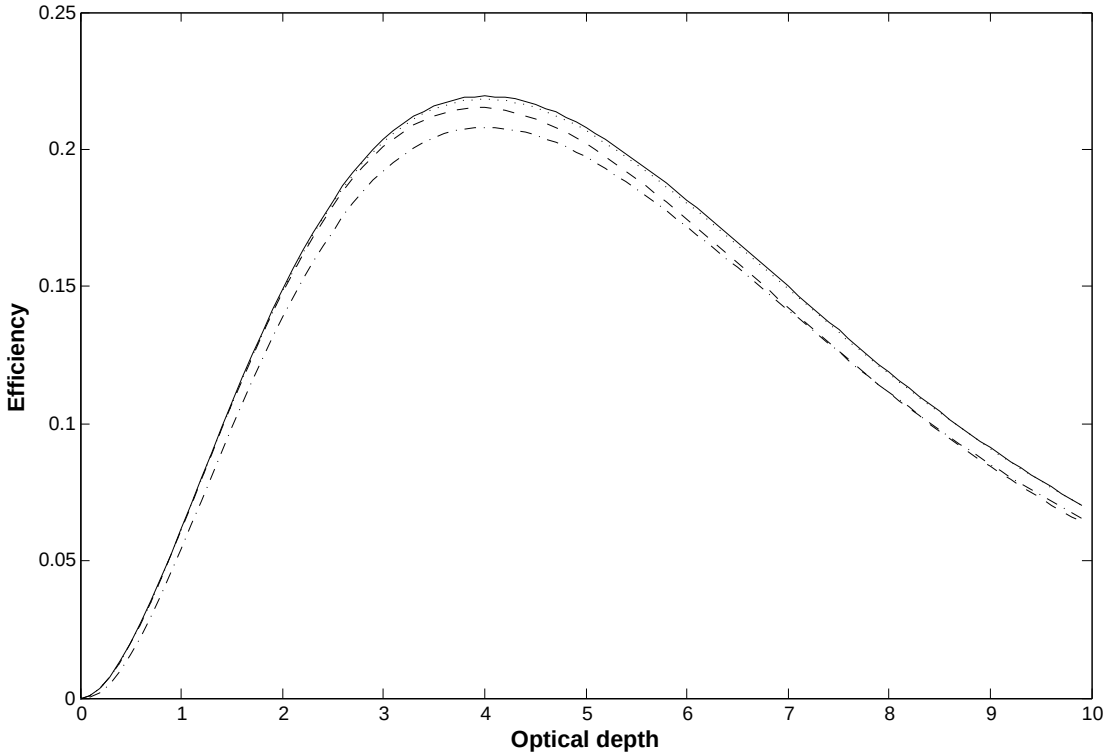

Figure 2.7: The efficiency of a square shaped AFC with a finesse of 2, a) Analytic result when $\Delta \ll \gamma_p \ll \Gamma$ (solid line). b) Numerical result with the aforementioned conditions (dotted line). c) $\Delta \ll \gamma_p$ holds and $\gamma_p = 0.5\ \Gamma$ (dashed line). d) $\gamma_p \ll \Gamma$ does hold and $\Delta = 0.5\ \gamma_p$ (dash-dotted line).

Chapter 3

CAVITY-ENHANCED AFC QUANTUM MEMORY

As mentioned in the last chapter, an AFC memory that acts like a plain frequency sampler (or filter) can have an efficiency of at most 54%. This can potentially be a serious issue for an application. For the quantum repeater scheme the problem is quite pronounced since the distribution rate sharply depends on the efficiency of quantum memories when a considerable number of elementary links are included in an implementation [1].

Employing a pair of Π pulses to map the collective excited state in equation 2.6 into a spin-state and then remap the state to another collective state is a technique that can in principle yield an efficiency of 100%. Under certain conditions, this technique causes the echo to be delivered in the backward direction and the altered dynamics removes the limitation of efficiency [8].

Unfortunately, the above scheme requires high optical depths (around 40) and high finesse ($F > 5$) in order to reach an efficiency of more than 90%. Making an AFC with these characteristics is quite demanding and the proposed scheme considerably increases the experiment's complexity.

Luckily, there exists a theoretical proposal [23] whereby enclosing an AFC crystal inside a judiciously chosen cavity allows the memory efficiency to be more than 90% at reasonable optical depths. In this chapter the theoretical material required to understand how a cavity-enhanced AFC memory works is reviewed. In addition, the efficiency is analytically calculated by considering experimental restrictions.

[1] Refer to equation 1.8.

3.1 Fabry-Pérot Cavity

3.1.1 The general dynamics

A Fabry-Pérot cavity is made of two parallel reflective surfaces. The dynamics of a Fabry-Pérot cavity with flat reflective surfaces (here and henceforth, we will refer to Fabry-Pérot cavity simply as "a cavity") is straightforward to derive, especially when the geometry is assumed to be one-dimensional. There exist various ways to derive the response function of a cavity in the frequency domain including the "sum over all round-trips" approach [11] and solving the set of equations that represents how the electric field amplitude gets reflected and transmitted at the interfaces [24]. The result gives the response function for transmission and reflection. By representing the reflectivity of the front surface as R_1 and the back surface by R_2, the corresponding transmissions as $T_i = 1 - R_i$ $\{i = 1, 2\}$, the reflection and transmission amplitudes as $r_i = \sqrt{R_i}$ and $t_i = \sqrt{T_i}$ and assuming the geometry to have just one dimension, the response functions for transmitted and reflected electric field amplitudes are

$$t_{cav} = \frac{t_1 t_2 e^{i\tilde{k}L}}{1 - r_1 r_2 e^{i2\tilde{k}L}} \ , \tag{3.1}$$

and

$$r_{cav} = \frac{r_1 - r_2 e^{i2\tilde{k}L}}{1 - r_1 r_2 e^{i2\tilde{k}L}} \ , \tag{3.2}$$

where $\tilde{k}$ is the wavenumber, which is generally complex, L is the cavity length, and the front surface is supposed to be at the origin ($x = 0$) and the back surface at $x = L$. The real part of $2\tilde{k}L$ is the phase gained by the field in each round trip and the imaginary part represents round trip loss and absorption. The corresponding transmission and reflection electric field amplitudes are derived by multiplying the input field by the above response functions. The response functions for the intensities are given by the squared norm of equations 3.1 and 3.2.

Since the atomic medium is placed between the cavity mirrors, for the purposes of this work, the amplitude and the intensity of light *inside* the cavity also have to be considered.

They can be readily derived by the "sum over all round-trips" approach. By denoting the distance to the front cavity surface as x the answer is [2]

$$E_{cav} = t_1 e^{i\tilde{k}x} \left(\frac{1 + r_2 e^{2i\tilde{k}(L-x)}}{1 - r_1 r_2 e^{2i\tilde{k}L}} \right) , \tag{3.3}$$

and the absolute value square of the above gives the corresponding response function with regard to intensities.

The nomenclature used for a simple cavity is also used for the cavity-enhanced quantum memory scheme. Equations 3.1 and 3.2 show that the transmission is maximum and the reflection is minimum when the round trip phase ($2k_r L$, which is the real part of $2\tilde{k}L$) is a multiple of 2π. In this case the cavity is said to be at resonance. The corresponding frequencies are given by $v_m = m\frac{c}{2nL}$, where m is an integer, n is the real part of the index of refraction and L can be set to be constant [24]. The interval between two resonances in the frequency domain is called the *Free Spectral Range*, which is abbreviated as FSR. The cavity *linewidth* is defined as the *Full With at Half Maximum* (FWHM) of the transmission profile at resonance and, from 3.1, it is given by [11]

$$\delta\nu = \frac{2(FSR)}{\pi} \arcsin\left(\frac{1 - r_1 r_2}{2\sqrt{r_1 r_2}} \right) , \tag{3.4}$$

where the cavity linewidth is depicted as $\delta\nu$. The cavity *finesse* is defined as the ratio of the cavity FSR to the cavity linewidth [3]. Finesse is sometimes thought of as the quantity that represents the cavity's "quality". This is due to some practical applications like frequency sampling for spectrum analyzing where a high finesse means less uncertainty of the frequency resolution [11].

Another general property of a cavity is that it can store energy. As one can see from equation 3.6, the light intensity inside a cavity can be much larger than the intensity of the input light. For example, figure 3.1 illustrates the scenario in which both mirrors [4] have

[2] See appendix B for the derivation.

[3] Not to be confused with the notion of AFC finesse.

[4] The word "mirror" in the literature sometimes refers to a 100% reflective surface. In this work by "mirror" we refer to a reflective surface in general, either partially or a 100% reflective.

reflectivities equal to 90%.

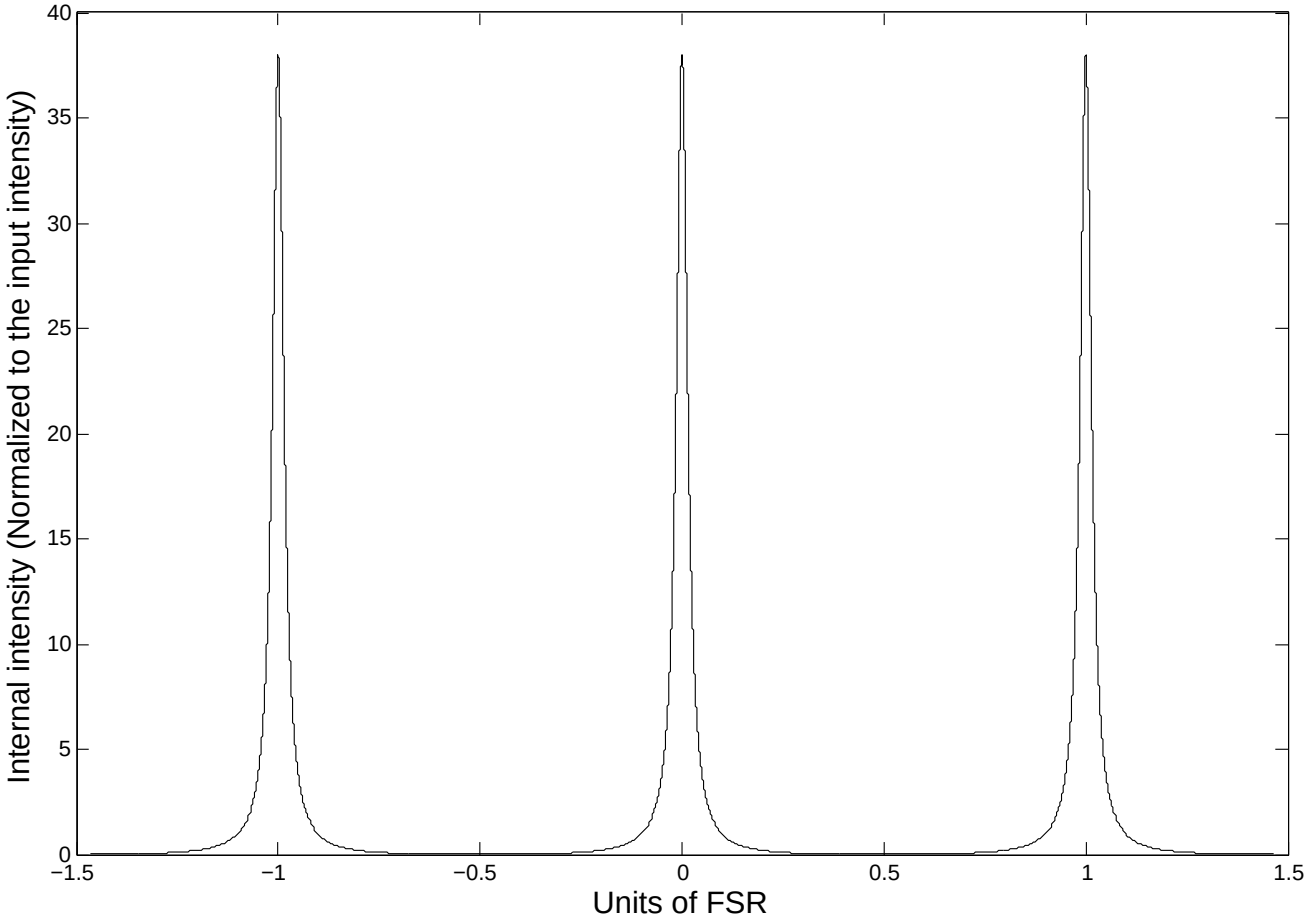

Figure 3.1: The scaled internal cavity intensity as a function of the cavity FSR when $R_1 = R_2 = 90\%$. The figure is derived using equation 3.6 , right after the front mirror and inside the cavity ($x = 0^+$). This point is arbitrarily chosen since the internal intensity depends on the position of the point that is studied.

The figure shows that the internal intensity at resonance is around 38 times larger than the input intensity. This phenomenon is used for enhancing the interaction of light with an atomic sample, but for implementing the cavity-enhanced AFC protocol it may add complications to an experimental implementation. This is because the intensity of burning pulses inside the cavity become highly non-uniform when they are sent through the cavity's

front surface. We will come back to this issue in chapter 6 .

3.1.2 Impedance matched cavity

For the AFC memory protocol with forward-direction retrieval, one of the main problems that leads to low memory efficiency is the non-zero probability of transmission (with no absorption) through the atomic medium. This is because the transmission probability follows the equation for transmission intensity $I_t = I_0 e^{-\tilde{d}}$, where I_t, I_0 and $\tilde{d}$ are transmitted intensity, input intensity and the average AFC optical depth respectively. The equation tells us that the directly transmitted light has an intensity that is reduced exponentially, by increasing the effective optical depth of the AFC ($\tilde{d}$). However as depicted in figure 2.7 there exists an optimum value for the optical depth. By further increasing the optical depth, the efficiency reduces due to re-absorption of the first echo in the medium [8] [5].

The dynamics of a cavity offers an effective and practical way for eliminating the light is transmitted through the crystal without being absorbed. From equation 3.2 the reflection intensity drops to zero when the cavity is on resonance and $R_1 = R_2 e^{-2k_i L}$ (k_i denotes the imaginary part of the wave number). The cavity is said to be *impedance matched* when R_1, R_2, cavity length, loss and absorption fulfill the relation $R_1 = R_2 e^{-2k_i L}$. One can send a pulse (or a photon) through the front mirror and have it be entirely absorbed by the medium. For example an AFC with average optical depth of 0.1 can be made 100% absorptive if the front mirror's reflectivity is set to 82% and the back mirror's reflectivity is set to 100%.

3.2 Cavity-enhanced AFC quantum memory

The idea of enclosing the memory with a judiciously chosen cavity in order to enhance the efficiency was first proposed in 2010 [23, 25]. Calculations in reference [23] show that by using this proposal high efficiencies can be reached by less demanding requirements than in

[5] Backward retrieval of the echo by utilizing a pair of Π pulses and a spin-state removes the mentioned restriction but, as stated at the beginning of this chapter, the requirements are challenging.

the case of a passive AFC or when spin-states and Π pulses are used for backward retrieval.

The general dynamics are derived by using the sum the "over all round-trips approach" and using the fact that the probability of absorption and re-emission by an atom have to be equal due to time reversal symmetry [21]. Also, it has to be noted that a photon may undergo an arbitrary number of round trips before being absorbed or re-emitted by the memory [23].

3.2.1 Calculation of efficiency

By following a similar procedure as in appendix B, the probability amplitude that a photon reaches an arbitrary point x inside the cavity while moving towards the back mirror is

$$\frac{\sqrt{T_1}e^{-(\alpha_0+\tilde{\alpha})x/2}e^{ikx}}{1-\sqrt{R_1R_2}e^{-(d_0+\tilde{d})}e^{2ikL}} \ , \tag{3.5}$$

where loss and absorption are separated from the real part of the wave number (k), the front mirror is placed at $x = 0$ and the back mirror at $x = L$. For half a round trip, loss and average AFC absorption are denoted as d_0 and $\tilde{d}_1$ respectively. In addition $\alpha_0 = \frac{d_0}{L}$ and $\tilde{\alpha} = \frac{\tilde{d}}{L}$.

Likewise, the probability amplitude that a photon gets re-emmited from an arbitrary point x inside the cavity and subsequently transmits through the front mirror after reflecting off the back mirror is

$$\frac{\sqrt{T_1R_2}e^{-\alpha_0(L-x)/2}e^{-\tilde{\alpha}(L-x)/2}e^{-(d_0+\tilde{d})/2}e^{ik(L-x)}}{1-\sqrt{R_1R_2}e^{-(d_0+\tilde{d})}e^{2ikL}} \ . \tag{3.6}$$

By using equatons 3.5 and 3.6 , the facts that the probability of absorption and re-emission at an element of the atomic medium is $\sqrt{\tilde{\alpha}}$ (see footnote 11 in chapter 2) and that the photon can get absorbed and re-emitted in either forward or backward direction, the efficiency of an cavity-enhanced AFC memory is given by

$$2\int_0^L \frac{\sqrt{T_1}e^{-(\alpha_0+\tilde{\alpha})x/2}e^{ikx}}{1-\sqrt{R_1R_2}e^{-(d_0+\tilde{d})}e^{2ikL}}\sqrt{\tilde{\alpha}}\sqrt{\tilde{\alpha}}\frac{\sqrt{T_1R_2}e^{-\alpha_0(L-x)/2}e^{-\tilde{\alpha}(L-x)/2}e^{-(d_0+\tilde{d})/2}e^{ik(L-x)}}{1-\sqrt{R_1R_2}e^{-(d_0+\tilde{d})}e^{2ikL}}\mathrm{d}x \ . \tag{3.7}$$

The result after considering the atomic dephasing due to the finite absorption linewidth is [6]

$$\sqrt{\mu} = \frac{2\tilde{d}e^{-(d_0+\tilde{d})}e^{ikL}T_1\sqrt{R_2\mu_f}}{\left(1-\sqrt{R_1R_2}e^{-(d_0+\tilde{d})}e^{2ikL}\right)^2} \ , \tag{3.8}$$

where μ_f and μ denote the atomic dephasing and the efficiency with respect to the intensities. The absolute square of the above is

$$\mu = \frac{4\tilde{d}^2e^{-2(d_0+\tilde{d})}T_1^2R_2\mu_f}{\left(1+R_1R_2e^{-2(d_0+\tilde{d})}-2\sqrt{R_1R_2}e^{-(d_0+\tilde{d})}\cos(2kL)\right)^2} \ . \tag{3.9}$$

From this formula it can be seen that the maximum efficiency is reached when the cavity is on resonance. Intuitively this is because at resonance the light that gets reflected from the front mirror of the cavity and hence *wasted* is minimum. In addition, when photons get re-emitted, they resemble hypothetical photons that have entered the cavity from the back mirror. Therefore the re-emitted photons will pass the front mirror by following the transmission profile, which is maximum at the resonance. For the rest of this chapter we assume that the cavity is on resonance.

The effective reflectivity of the back mirror is defined as $\bar{R}_2 = R_2e^{-2d_0}$. In the frame of an observer who can perform measurements just outside the front mirror (R_1), there is no way to distinguish between actual transmission through the back mirror and the intra-cavity loss. Therefore, the effective back mirror reflectivity would be a more relevant quantity than the actual back mirror reflectivity and the intra-cavity loss [7]

By employing the definition of the effective back mirror reflectivity and setting $\bar{R}_2 = 1$, $\sqrt{R_1} = 1-\epsilon$ with $\epsilon = \tilde{d} \ll 1$, equation 3.9 yields $\mu = \mu_f$ [23]. It shows that for a loss-less impedance matched cavity, the efficiency would be just limited by the intrinsic dephasing factor if the enclosed AFC has a low average optical depth.

[6] These calculations are similar to that performed in reference [23]. Nevertheless, we generalized the case to an arbitrary round trip phase e.g. the cavity can be on or off resonance. The main reason is to accomodate for experimental uncertainties in setting the frequency on resonance with the cavity.

[7] It is assumed that the intra-cavity loss is almost constant at the frequencies of light used in the experiment.

3.2.2 Optimizing the efficiency

The conditions that lead to the conclusion drawn so far are hard to be met experimentally. In fact none of the experiments performed so far [26, 27] or the one performed for completing this thesis, fulfilled the stated conditions. Accordingly, it is informative and instructive to investigate the circumstances that lead to maximum efficiency in a general case (i.e. arbitrary intra-cavity loss and AFC optical depth) . Impedance matching is not necessarily the optimum condition as is shown in this subsection.

Equation 3.8 (or 3.9) contains all the required information. Loss (d_0) generally depends on the material and often technical limitations (e.g. imperfect mode matching), and once optimization efforts are made, is constant during the course of any experiment. Any reduction of R_2 from unity would be a source of loss and so the back mirror has to be a perfect mirror. R_1 is typically a variable which is set beforehand by calculating the optimized value using the estimations of loss and absorption. The more flexible variable in 3.8 however is $\tilde{d}$ which may be tuned by changing the laser's wavelength[8] to optimize the efficiency for some value of loss and front mirror's reflectivity. Another way to adjust the value of $\tilde{d}$ is changing the AFC finesse. Nevertheless, changing the finesse is less straight forward as it can be limited by spectroscopic properties of ions being used. From this point I assume the AFC finesse to be a constant.

When R_1 is the variable parameter, its optimum value is found by taking the derivative of equation 3.8 with respect to R_1 and setting it equal to zero. The result confirms that in this case the efficiency is maximized when $R_1 = R_2 e^{-2(d_0+\tilde{d})} = \bar{R}_2 e^{-2\tilde{d}}$, which is the impedance matching condition. By putting this value of R_1 in equation 3.8 we get

$$\sqrt{\mu} = \frac{2\tilde{d}e^{-\tilde{d}}\sqrt{\bar{R}_2\mu_f}}{\left(1-\bar{R}_2 e^{-\tilde{d}}\right)} \ , \tag{3.10}$$

which in comparison to a bare crystal (a crystal that is not not inside a cavity) with length

[8] It is arguably assumed that absorption is negligible at the transmission windows that are made in order to carve the AFC.

$2L$ [9], shows an enhancement factor of $\left(1-\bar{R}_2 e^{-\tilde{d}}\right)^{-1}$ which has a minimum value equal to one [10] .

The situation is considerably different when d is variable and R_1 is constant. In this case the extrema is optained when

$$\sqrt{R_1 \bar{R}_2} e^{-\tilde{d}} = \frac{1-\tilde{d}}{1+\tilde{d}} \ , \tag{3.11}$$

which does not satisfy the impedance matching condition. The value of $\tilde{d}$ that satisfies 3.11 is between 0 and 1. It can be justified by looking at equation 3.8 (which quantifies the efficiency of a cavity enhanced AFC) and comparing it with equation 2.7 (which quantifies the efficiency of a bare AFC). In equation 3.8 the numerator $2\tilde{d}e^{-\tilde{d}}T_1\sqrt{\tilde{R}_2\mu_f}$ represents the efficiency of an AFC with length $2L$, which is reduced by the T_1 factor due to input and output transmissions through the front mirror. Since $\tilde{d}$ is the only variable, the numerator is maximum when $\tilde{d}=1$ as in the case of a typical AFC with length $2L$. The reciprocal of the denominator of 3.8 represents the square of the sum over all round trips for the photon's probability amplitude. When R_1 and $\bar{R}_2$ are constant this term is maximum when $\tilde{d}=0$. Correspondingly the maximum value of 3.11 happens when $0 \leq \tilde{d} \leq 1$.

When $\tilde{d}$ and loss are much smaller than one, which is the case considered in the last section of [23] ($\tilde{d}$ is set to be 0.1 and loss is assumed to be zero) the optimum optical depth from equation 3.11 converges to the impedance matching condition. In this case 3.11 can be written as

$$\sqrt{R_1} e^{-\tilde{d}} \simeq \frac{e^{-\tilde{d}}}{e^{\tilde{d}}} \ , \tag{3.12}$$

and it follows that

$$\sqrt{R_1} \simeq e^{-\tilde{d}} \ . \tag{3.13}$$

which is the impedance matching condition. In the experiment explained in this thesis,

[9] $2L$ is the effective length of the crystal when $R_2=1$ and $R_1=0$.

[10] Setting $R_1=0$ and $R_1=1$ results in the efficiency to be one or zero respectively, in units of a bare AFC efficiency with length $2L$. There exists just one exterma for 3.8 and it is larger than one in unit of the bare AFC efficiency. Thus the extremum is indeed a maximum.

neither loss nor $\tilde{d}$ are small so looking for the impedance matching condition would have been a mistake.

Chapter 4

THE EXPERIMENT

The cavity enhanced AFC memory scheme has been successfully implemented in [26] and [27] and efficiencies of 56% and 53% were reported, respectively. In [27] a slab of bulk crystal with a slight wedge on one side was partially reflection coated on the wedged side and high reflection coated on the other side to make the cavity impedance matched while having the freedom to move the resonance in the frequency domain. In [26] the crystal was inside an external cavity which was longer than the crystal's length to have the freedom to apply pulses that prepared the AFC at a small angle with the cavity axis and have them unaltered by the cavity profile.

In our experiment, a waveguide crystal was used. It's back surface was 100% reflection coated and the difference of the index of refraction of the crystal and vacuum provided the front mirror of the cavity with 14% reflectivity. In this chapter the experimental setup and basic measurements of loss and atomic absorption are described.

4.1 The experimental setup

The rare-earth ion doped crystal in the experiment was thulium doped lithium niobate $Tm : LiNbO_3$. The waveguides have been fabricated inside the crystal by in-diffusing titanium [28].

The crystal contains several groups of waveguides which each contain ten waveguides, with diameters ranging from 2.5 μm to 7 μm in increments of 0.5 μm. The width of each group is 1 mm and the distance between two adjacent waveguides is 0.1 mm. Figure 4.1 portrays the waveguides and their geometry.

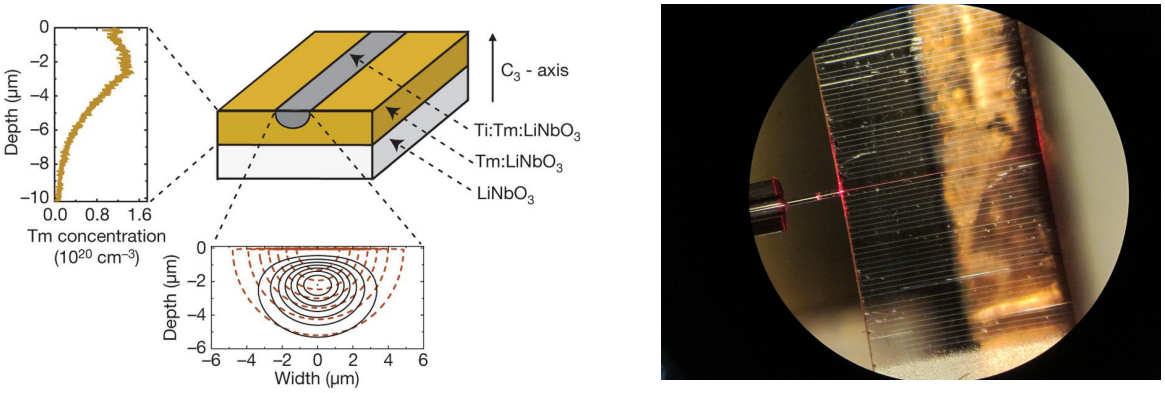

Figure 4.1: Left: Waveguide geometry. The measured thulium (Tm) concentration profile is given on the left and the calculated intensity distribution at the 795-nm wavelength is shown below. Iso-intensity lines are plotted corresponding to 100%, 87.5%, 75% and so on of the maximum intensity (Figure and caption taken from [1]). Right: Waveguide groups. Waveguide groups and individual waveguides are seen in this picture, which was taken under a microscope. One of the waveguides was illuminated using a red laser and a fiber to couple the light into the waveguide.

The crystal thickness is 0.5 mm and the width (perpendicular to the waveguides) is around 1 cm. The length of the two used crystals (parallel to the waveguides) is 2 mm or 5 mm. Unlike the back surface, which is high reflection coated, the front surface of the crystal is not reflection coated. Nevertheless the difference between the indexes of refraction of the crystal and vacuum causes it to have an effective 14% reflectivity. Likewise the front surface of the fiber that is used for coupling the beam into waveguides has an effective 4% reflectivity. The experimental layout is shown in figure 4.2.

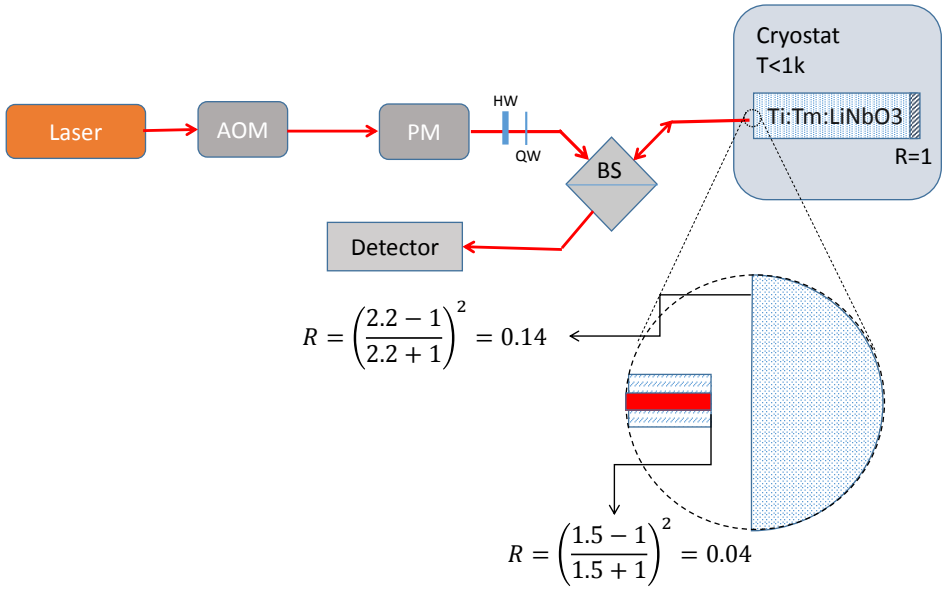

Figure 4.2: The setup. A diode laser provides a beam at around 795 nm wavelength and the Acousto-Optic Modulator (AOM) carves the required pulses out of it. The Phase Modulator (PM) is used to shift the frequency when required and make the scan in frequency domain to read out the absorption spectrum. The Half-Wave plate (HW) and the Quarter-Wave plate (QW) set the polarization of the light to maximize or minimize the interaction of light with thulium atoms. The Beam Splitter (BS) makes it possible to send the cavity response to a detector without being mixed with the input light.

The crystal is in a cryostat that cools down to 0.7 Kelvin and so phononic perturbations are minimized and allow for a narrow homogeneous linewidth. A 50-50 beamsplitter is used to separate the cavity response from the input beam and pulses.

4.2 Coupling the fiber to waveguides

The fiber can move towards or away from the crystal by using a piezoelelectric translation stage. The stage can also move the fiber horizontally or vertically with respect to the crystal front face. The corresponding axes are named X, Y and Z. The layout of the fiber and crystal

is shown in figure 4.3.

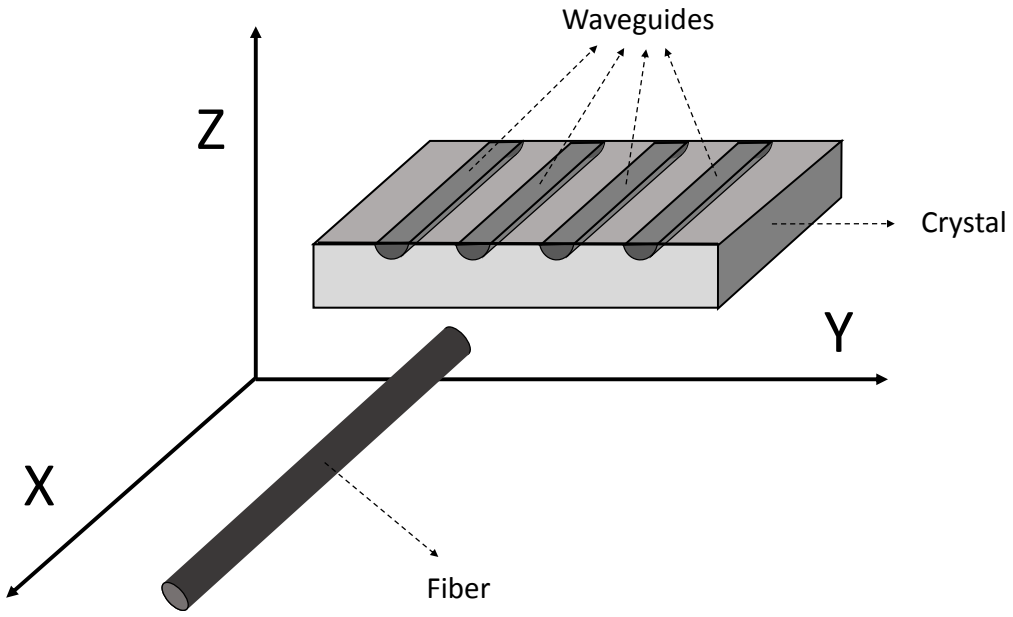

Figure 4.3: The layout of the fiber and crystal (not in scale). A piezeoelelectric translation stage moves the fiber in the X, Y and Z directions. The crystal is mounted on a stationary stage (not shown).

Coupling the fiber to a waveguide is done by setting the position of the fiber along all three axes such that it is in front of a waveguide and close to the crystal surface or touching it. Since the crystal is just 0.5 mm thick the first step of the alignment is to put the fiber in front of the crystal by moving it in the Z direction. When the fiber is above the crystal (or too far from it in the X direction), just 4% of the input beam is reflected (from the fiber surface) and what is not reflected is lost. When the fiber is level with the crystal's upper surface (and not too far from it in the X direction) a jump in the amount of reflected light can be seen, since some of the light that is transmitted through the fiber can be reflected back from the crystal surface and into the fiber. Another sign of the fiber being in front of

the crystal is fluctuations in the detected light, which are caused by pumping of the cryostat and other sources of vibration [1].

The alignment in the X direction can be tracked by following the reflected light pattern when the fiber moves towards the crystal. When the fiber is not in front of a waveguide, a cavity will form between the fiber surface and crystal front surface. This is dubbed the *secondary cavity* to be distinguished from the cavity made by the crystal (main cavity). Using the 4% and 14% reflectivities, equation 3.2 gives the maximum and minimum normalized reflection intensities from the secondary cavity as 3.5% and 28.5%. The round trip phase (phase that electric field gains in a round trip) changes periodically when the cavity length (distance between fiber and crystal surfaces) changes. More precisely, the phase acquired in one round trip is equal to $2kL$ where k is the (real) wavenumber and L represents the length of the secondary cavity. When the wavelength is almost constant, L determines the phase. Putting $2kL = 2m\pi$ where m is an integer shows that the successive maxima (or minima) occur at multiples of $\lambda/2$ where λ is the wavelength. When the fiber starts touching the crystal the cavity pattern starts to fade away up to a point where the fiber can not move in further.

At around 795 nm the interval between successive maxima (or minima) happens at less than 400 nm, so the round trip phase can readily be changed by adjusting the cavity length. Adjusting the round trip phase by modifying the frequency of the laser on the other hand is not feasible. A simple calculation shows why. The secondary cavity's FSR is equal to $\frac{c}{2L}$ in which c is the speed of light. The finesse is roughly two, so the cavity linewidth reads $\delta\nu = \frac{c}{4L}$. Since the fiber core diameter is a few microns, we may roughly assume that distance between the fiber and crystal should be of the same order for the beam divergence to be small. If we plug in $L = 10\ \mu m$ in the former formula we get $\delta\nu = 10\ THz$. In all measurements in this experiment variation of frequency has been at least two orders

[1] Vibrations slightly change the configuration of the cavity formed between the fiber and crystal front surface. Therefore, the light that gets reflected back to the fiber fluctuates in intensity.

of magnitude smaller than the above number. Henceforth when frequency is the quantity subject to change, the secondary cavity is almost static (it's response does not change with time).

Alignment in Y direction is done after making sure that the fiber is close to the crystal and the fiber is level with the crystal's upper surface (that includes the waveguides). The used method in the experiment to find the waveguides is to have the burning cycle on and then readout the response in the frequency domain by a scan. When the effect of hole burning is seen in the reflection profile, we are sure that the fiber is aligned to a waveguide.

4.3 Hole burning

The first use of hole burning in the experiment is to make sure that the light interacts with atoms i.e. that it is coupled into a waveguide. As explained in chapter 2, when the pumping interval or sequence of pumping pulses are long and strong enough, atoms are expected to be removed from the ground state and provide a transparent window in the absorption spectrum. The hole alters the cavity response and it's existence can be detected through the alteration of the frequency dependence of the reflected light. The following picture is an example of hole burning in the $5mm$ long crystal.

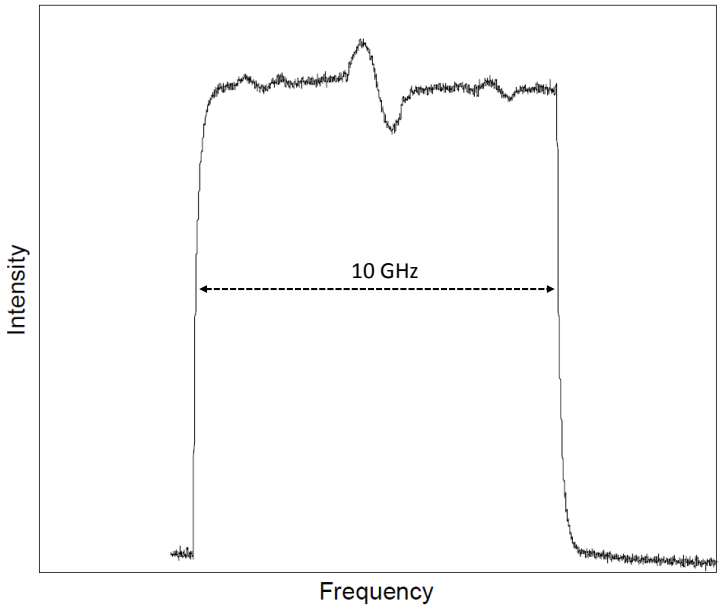

Figure 4.4: The reflection response after hole burning in a $5mm$ long cavity. At the middle of the scan range the cavity response can be seen as a result of the transparent interval which was around 1GHz wide. The theoretical value for the Free Spectral Range (FRS) is around 14 GHz but in the above picture it is reduced to 2 GHz due to a strong slow light effect (see appendix C). The measurement was done at 792.8 nm.

At later stages of the experiment we used the $2mm$ long crystal and its smaller loss resulted in a stronger signal and a more dramatic alteration of the reflection profile. This is shown in figure 4.5.

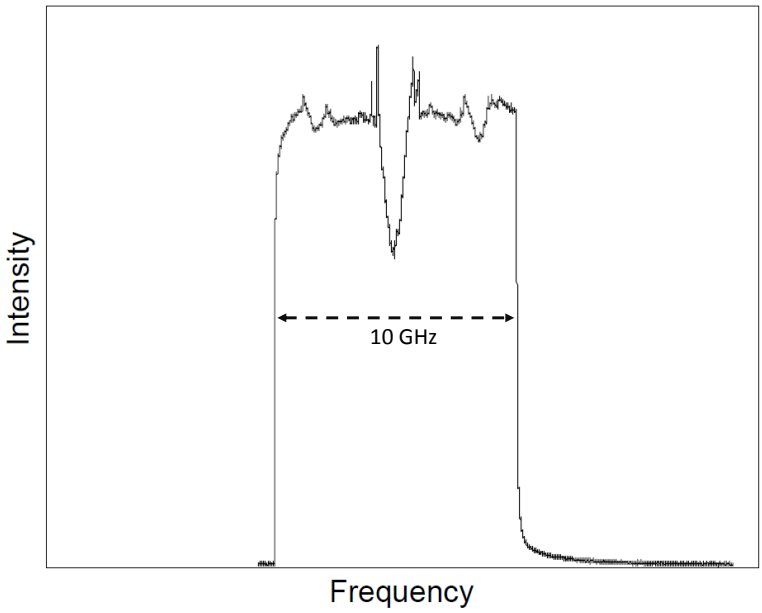

Figure 4.5: The reflection response after hole burning in a $2mm$ long cavity. At the middle of the scan range, the cavity response can be seen as a consequence of the transparent trench (around 1GHz wide). Edges of the hole show an increase in intensity and the slow light effect caused the cavity response to be "squeezed" inside the hole. The theoretical value for the Free Spectral Range (FSR) is around 35 GHz and unlike the $5mm$ crystal shown in figure 4.4, the slow light effect is not strong enough to observe a minimum *and* a maximum. The measurement is done at 794.3 nm.

4.4 Loss and absorption measurements

4.4.1 Loss measurement

A critical quantity for the performance of the cavity enhanced AFC is the internal loss inside the cavity. As seen in equation 3.11 and discussions later in chapter 3 , loss shifts the optimum condition from impedance matching for a dynamic AFC [2]. For a static AFC [2] in contrast, impedance matching is the optimum condition but loss can converge the gain in

[2] In this manuscript, a "dynamic" AFC or cavity refers to an AFC or a cavity with variable factors. Likewise, a "static" AFC or cavity refers to an AFC or a cavity with constant factors.

efficiency to zero according to equation 3.10.

Loss evaluation can be done by measuring the cavity response outside the atomic resonance. To that end, a measurement is done at 800 nm, which is far from the resonance wavelength. The polarization is the same as that, which at around 795 nm wavelength maximizes the interaction with the atoms. Another measurement is performed when the wavelength is 794.6 nm (resonant wavelength), but with the polarization set not to interact with the atoms. In a first approximation, the reflection from the fiber's front surface can be ignored. Therefore, the secondary cavity can be ignored as well [3]. In this approximation, from equation 3.2, the maximum and minimum normalized intensities reflected from the cavity are

$$\begin{aligned} I_{max} &= \alpha^2 \left| \frac{r + r'}{1 + rr'} \right|^2 \\ I_{min} &= \alpha^2 \left| \frac{r - r'}{1 - rr'} \right|^2 \end{aligned} \quad , \tag{4.1}$$

where α is the coupling coefficient, which is assumed to be equal for the input to and output from the waveguide. Setting $r = \sqrt{0.14}$ as the front mirror's reflectivity, $1 - |r'|^2$ represents loss in the medium. Equation 4.1 provides two equations using which r' and α can be derived by measuring the values of I_{max} and I_{min}. At 800 nm the measured values are $I_{max} = 0.24$ and $I_{min} = 0.06$ [4] yielding $\alpha = 0.58$ and $r' = 0.69$. At 794.6 nm and "off resonant" polarization, the measured values are $I_{max} = 0.09$ and $I_{min} = 0.02$. They give two sets of solutions, which are $\alpha = 0.59, r' = 0.17$ and $\alpha = 0.37, r' = 0.64$. Since coupling should not depend strongly on polarization, the first set is regarded as the physical answer. The smaller value of r' in comparison to the measurement at 794.6 nm is due to the fact that waveguide loss is polarization dependent and when the polarization is "off resonant" with the atoms, loss in the waveguides is maximum [28].

Loss should not change dramatically with wavelength so we can assume that the values

[3] The acquired round trip phase for the secondary cavity was almost the same in both cases, since $\Delta\phi = 2kL = \frac{4\pi}{\lambda}L$, L was constant and λ did not considerably differ.

[4] The normalization was done to the intensity of the beam that reflects off the front surface of fiber (4 % of the input intensity) when it was not in front of the crystal.

derived for 800 nm also represent waveguide loss and coupling loss in the system when polarization is "on resonance" with the atoms.

In the experiments performed in [26] and [27] the efficiency could have been 84% and 85%, assuming square shaped AFCs and a lossless cavity. In practice the efficiency reduced to 56% and 53%, respectively. Plugging the values that are reported in those papers for the absorption optical depth, AFC finesse, and cavity surface reflectivities, into equation 3.8 shows that round trip loss in both experiments had an optical depth of less than 0.07. Unfortunately the intracavity loss is considerably larger in our experiment.

4.4.2 Absorption measurement

By using the same procedure as in the preceding section, we could measure the optical depth of the thulium atoms. The experiment was done at 794.6 nm, which we empirically found to be the wavelength that delivers the maximum memory efficiency. The normalized maximum and minimum reflection intensities were measured to be 0.066 and 0.035 respectively. Plugging these values into 4.1 delivers two sets for the unknowns α and r': $0.60, 0.07$ and $0.28, 0.84$. Since the loss measurements described in the former subsection gave $\alpha \simeq 0.58$, the first set is the physical answer. The corresponding absorption plus loss optical depth in the medium is $d_1 + d_0 = -\ln(0.07) = 2.66$. By subtracting the loss that was derived for the measurement at 800 nm, absorption is found to have an optical depth equal to 2.35 for the crystal with $2mm$ length at 794.6 nm.

Chapter 5

THE COMPOUND CAVITY ENHANCED AFC QUANTUM MEMORY

In the last chapter the effect of the fiber's front surface reflectivity was ignored when calculating loss and absorption inside a waveguide. Even though the relatively small value of the reflection (4%) makes that approximation justifiable, the discussions in section 4.2 suggest that, since the cavity formed between the fiber surface and the crystal's front surface has a reflectivity between 3.5% and 28.5%, it might have a significant impact on the dynamics. In addition, during the course of experiment, we observed some behavior depended on the distance between the fiber and the crystal that seemed incomprehensible at first. We observed that when the fiber that coupled the light into the cavity moved toward or away from the front surface of a waveguide, the cavity resonance slightly moved in the frequency domain. Some study and calculations revealed that the investigated system was in fact a compound cavity with three reflective surfaces: the front and back surfaces of the crystal plus the end surface of the fiber.

In this chapter the calculations that show how this compound cavity responds to input light are presented. The way that it affected our experiment and how it can be used to increase efficiency of an AFC quantum memory is also discussed.

5.1 The general dynamics

Solving the equation set that is obtained by considering the electric field that gets reflected and transmitted through each mirror provides a straightforward but somewhat cumbersome way to derive the dynamics of a compound cavity. When three mirrors are involved, the

situation looks like that sketched in figure 5.1 .

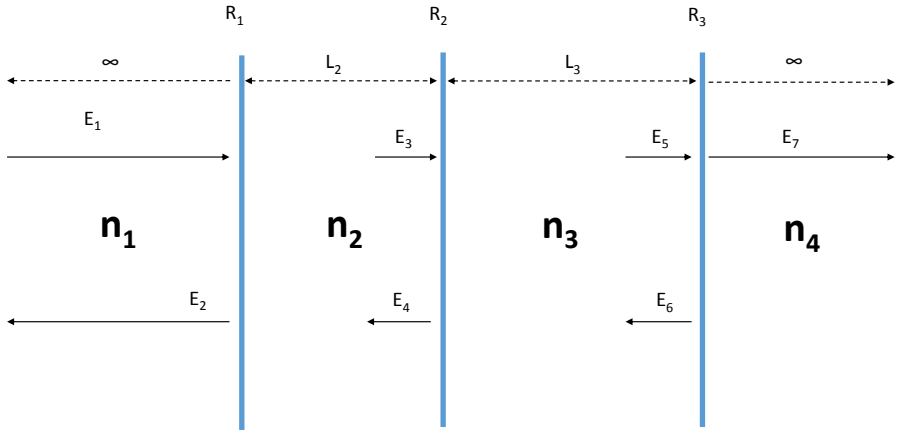

Figure 5.1: A sample compound cavity with three mirrors. E_1, E_2 and E_7 are the input, reflected and transmitted amplitudes of the combined system, respectively. All electric fields correspond to values right before or after the reflective surfaces. The indices of refraction are indicated by n_i.

By assuming that $n_2 < n_1, n_2 < n_3$ and $n_4 < n_3$, which was the case for our experiment,

the following set of equations emerge from the Fresnel relations for each surface[1]

$$\begin{aligned} E_2 &= r_1 E_1 + t_1 E_4 e^{ik_2 L_2} \\ E_3 &= t_1 E_1 e^{ik_2 L_2} - r_1 E_4 e^{i2k_2 L_2} \\ E_4 &= t_2 E_6 e^{ik_3 L_3} - r_2 E_3 \\ E_5 &= t_2 E_3 e^{ik_3 L_3} + r_2 E_6 e^{i2k_3 L_3} \\ E_6 &= r_3 E_5 \\ E_7 &= t_3 E_5 \quad , \end{aligned} \tag{5.1}$$

which are six equations and six unknowns.

The solution to this set of equations for the reflected ($E_r = E_2$) and transmitted ($E_t = E_7$) electric field amplitudes divided by the input amplitude ($E_i = E_1$) gives the reflection response as

$$r = \frac{-r_1 + r_1 r_2 r_3 e^{i2k_3 L_3} - r_3 e^{i2k_3 L_3 + i2k_2 L_2} + r_2 e^{i2k_2 L_2}}{1 - r_2 r_3 e^{i2k_3 L_3} + r_1 r_3 e^{i2k_3 L_3 + i2k_2 L_2} - r_1 r_2 e^{i2k_2 L_2}} \ , \tag{5.2}$$

and the transmission response

$$t = \frac{\left(t_1 t_2 t_3 e^{ik_2 L_2 + ik_3 L_3}\right)}{\left(1 - r_2 r_3 e^{i2k_3 L_3} + r_1 r_3 e^{i2k_2 L_2 + i2k_3 L_3} - r_1 r_2 e^{i2k_2 L_2}\right)} \ . \tag{5.3}$$

The validity of the above relations is confirmed by checking the limiting cases of $r_i = 0$ and $r_i = 1$. For instance, putting $r_3 = 0$ reduces 5.2 and 5.3 to the reflection profile and transmission profile of a bi-mirror cavity with reflection amplitudes r_1 and r_2. Conservation of energy is a further confirmation that equations 5.2 and 5.3 are valid.

Paying close attention to equations 5.2 and 5.3 and the limiting cases shows that the three-mirror cavity is effectively a "superposition" of three bi-mirror cavities. These cavities are formed by mirror couples $\{r_1, r_2\}$, $\{r_2, r_3\}$ and $\{r_1, r_3\}$. In fact, letting the reflectivity of one of the mirrors approach zero reduces the case to the problem of a single cavity, which is "perturbed" by the existence of two other cavities.

[1] Specifically we are considering the case that $n_2 = n_4 = 1$, so the possible lack of knowledge about the structure of reflection coatings does not lead to any confusions about the acquired phases on reflections. Reflections from the vacuum side leads to a π phase shift, so the beam that comes toward the vacuum side acquires a zero phase shift.

Loss and absorption that occurs between the first and second, or the second and third mirror can be taken into account by regarding k_2 and k_3 to be complex. In this case they are denoted as $\tilde{k}_2$ and $\tilde{k}_3$.

5.2 The compound cavity enhanced AFC quantum memory

5.2.1 Resonance of compound cavity

The first thing to note in studying a compound cavity-enhanced AFC quantum memory is that Eqs. 5.2 and 5.3 do not require the maximum absorption to take place at the resonance of the main cavity (formed by R_2 and R_3) or the secondary cavity (formed by R_1 and R_2). This is because the dynamics is given by the "superposition" of three cavities, as pointed out above. For example, numerical calculations with MATLAB show that putting $R_1 = 0.1$, $R_2 = 0.14$ and $R_3 = 0.3$ requires $k_2L_2 = 0.6271\pi$ and $k_3L_3 = 0.1359\pi$ to maximize the absorption of the compound cavity. The minimum absorption is, however, found in the lab empirically by scanning the phases acquired in each round trip of the main and the secondary cavity. This explains the observation that by moving the fiber toward or further away from the crystal, the "resonance" appears to be moving periodically in the frequency domain. Changing the phase acquired in each round trip of the secondary cavity by changing it's length makes the maximum absorption happen at a frequency that is not exactly the one at which the main cavity is on resonance[2]. Consequently the compound cavity resonance changes by changing the round trip phase of the secondary cavity. Figure 5.2 illustrates this phenomenon.

[2]As explained in chapter 4, the short length of the secondary cavity in the experiment made it's profile practically unalterable when the frequency was modified.

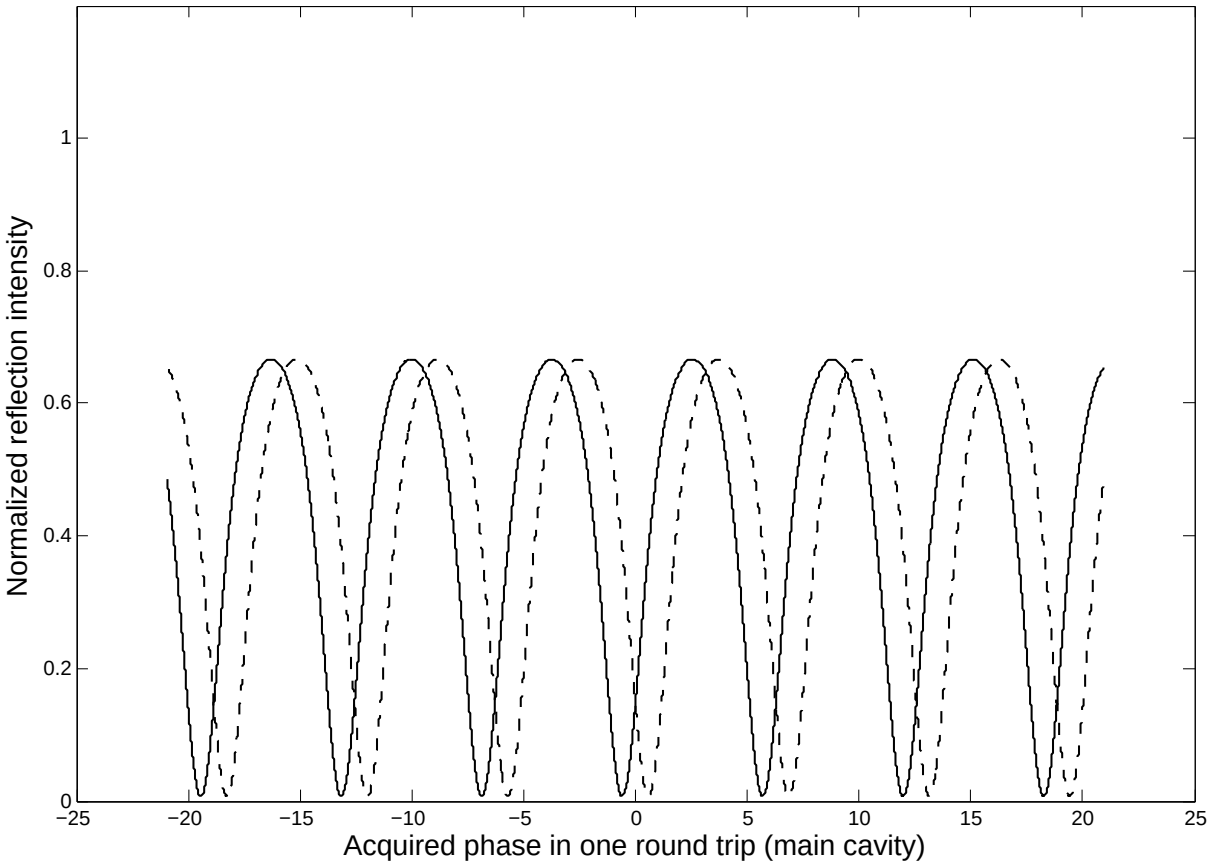

Figure 5.2: For a compound cavity the maximum absorption does not necessarily happen at the resonance of the cavity formed by the couple of mirrors that enclose the absorptive crystal. In this figure the mirror reflectivities are set to $R_1 = 0.1$, $R_2 = 0.14$ and $R_3 = 0.3$. The broken line shows the case if the phase acquired in one round trip for the secondary cavity is $\pi/2$ and the solid line when the phase is $-\pi/2$.

In [29] the crystal had a small wedge in order to allow modifying the resonance frequency of the cavity. It consequently increased the loss inside the cavity, due to the beam walk-off as the beam bounced between the mirrors. The above phenomenon provides an alternative approach for modifying the cavity resonance.

5.2.2 Finding the impedance matching condition and making an AFC

Impedance matching is *not* generally the optimum condition when a static[3] cavity is used to enhance the efficiency of a dynamic AFC[3] memory as stated in chapter 3 section 3.2. However, it *is* the optimum condition for the case in which loss and average optical depth of the absorption ($\tilde{d}$) are much smaller than one or when the cavity is dynamic and the AFC is static. Furthermore, the fact that burning, readout and possible control beams get altered by the cavity profile may add serious complications in making an optimum AFC inside a cavity. Compound cavity dynamics provides a way to find the impedance matching condition and burn an AFC, which is (at least theoretically) quite straight forward.

Equation 5.2 reveals that when $R_2 = R_3$ (the main cavity is impedance matched[4]) and $2k_3L_3$ is a multiple of 2π (the main cavity is on resonance), the reflection profile reduces to $r = -r_1$ and any further effect of the secondary cavity is eliminated. Intuitively this is because when the main cavity is on resonance and impedance matched, it absorbs (or transmits) the whole input intensity, therefore no photon that passes through R_1 will be able to find its way back to R_1, and the compound cavity's reflection will be just equal to the reflectivity of R_1.

Likewise, when $R_1 = R_2$ and $2k_2L_2 = 2m\pi$, which represent the case in which the secondary cavity is on resonance and symmetrical, the reflection profile reduces to $r = -r_3$ and any further effect of the main cavity gets eliminated. Intuitively this is because when the secondary cavity is on resonance and symmetrical, it will pass the whole input intensity and when a portion of this beam gets reflected from R_3 back to R_2 and R_1, all of it passes through the secondary cavity, again since it is on resonance and symmetrical.

The first scenario can be used to make sure that the cavity that includes the crystal (the main cavity) is impedance matched, for example by using a bare fiber with a surface that

[3] For definition of "dynamic" and "static" look at the footnote in page 42.

[4] For the purpose of this subsection we regard a reduction of R_3 from one to represent loss plus absorption in the main cavity. In addition, we assume the secondary cavity to be lossless.

is properly reflection coated and moving it toward or further away from the main cavity. The second scenario, on the other hand, provides a way to send in burning, readout and possible control beams to the crystal from the front surface to make the AFC and read it out, without getting affected by the cavity structure.

5.2.3 Calculation of efficiency

Guided by the way the efficiency of a regular (not compound) cavity-enhanced AFC is derived analytically (refer to section 3.2) the efficiency of a compound cavity-enhanced AFC can also be found. In equation 5.3 the numerator is shared between all possible pathways inside the compound cavity that lead to transmission through R_3. Therefore the denominator must represent the sum over all round trips. For the purpose of analysis in this subsection, we regard r_3 to represent just the back mirror's reflectivity. The effect of loss in the secondary cavity and main cavity may be taken into account by replacing k_2 and k_3 with the complex counter parts $\tilde{k}_2$ and $\tilde{k}_3$.

We denote the denominator of 5.3 as

$$D = \left(1 - r_2 r_3 e^{-\tilde{\alpha} L_3} e^{i2k_3 L_3} + r_1 r_3 e^{-\tilde{\alpha} L_3} e^{i2k_2 L_2 + i2k_3 L_3} - r_1 r_2 e^{i2k_2 L_2}\right) \ . \tag{5.4}$$

Similar to 3.8 we get for the efficiency

$$\sqrt{\mu} = 2 \int_0^{L_3} \frac{t_1 e^{ik_2 L_2} t_2 e^{ik_3 x_3} e^{-\tilde{\alpha} x_3/2}}{D} \tilde{\alpha} \frac{t_1 e^{ik_2 L_2} t_2 e^{ik_3 (L_3 - x_3)} r_3 e^{-\tilde{\alpha} L_3/2} e^{ik_3 L_3} e^{-\tilde{\alpha}(L_3 - x_3)/2}}{D} \sqrt{\mu_f} dx_3 \ , \tag{5.5}$$

and the result is

$$\sqrt{\mu} = \frac{e^{i2(k_2 L_2 + k_3 L_3)} 2\tilde{d} e^{-\tilde{d}} T_1 T_2 r_3 \sqrt{\mu_f}}{\left(1 - r_2 r_3 e^{-\tilde{\alpha} L_3} e^{i2k_3 L_3} + r_1 r_3 e^{-\tilde{\alpha} L_3} e^{i2k_2 L_2 + i2k_3 L_3} - r_1 r_2 e^{i2k_2 L_2}\right)^2} \ , \tag{5.6}$$

where μ_f represents the atomic dephasing and $\tilde{d} = \tilde{\alpha} L_3$ is the average optical depth of the AFC. This equation reduces to Eq. 3.8 when T_1 or T_2 is set to one. The absolute value square of the above gives the efficiency in terms of intensities.

Equation 5.6 corresponds to the probability that 1) a photon enters the compound cavity through the front mirror (R_1) and reaches an arbitrary point inside the main cavity, 2) gets absorbed, 3) is retrieved, and 4) passes the front mirror of the compound cavity. The first and fourth stages are directly dependent on the sum over all round trips. This is also true for the transmission profile in equation 5.3. Consequently, when the transmission is maximum, the absorption is maximized and conservation of energy requires reflection to be minimum. As a result, when the round trip phases make the reflection of the compound cavity minimum, the efficiency is maximum, irrespective of the loss in the main and the secondary cavities.

5.3 The compound cavity in the experiment

For our experiment, $R_1 = 0.04$ is the reflectivity of the fiber surface due to difference between its index of refraction and that of vacuum. Likewise, $R_2 = 0.14$ is the reflectivity of the front surface of the crystal due to differences in indices of refraction of lithium niobate and vacuum. The back surface of the crystal is 100% reflection coated. The waveguide crystal loss, which is placed between R_2 and R_3, is calculated in the previous chapter under the approximation that R_1 is negligible. The coupling loss between the fiber and waveguide is also calculated using the same approximation. If R_1 is not set to zero, coupling loss can be represented as loss inside the secondary cavity.

The following figure depicts the numerically calculated reflection profile of the considered experiment's compound cavity by assuming the loss inside the main cavity and secondary cavities to be those that were calculated in the previous chapter which yield loss optical depth in half round trip to be 0.37 for the main cavity and 0.53 for the secondary cavity.

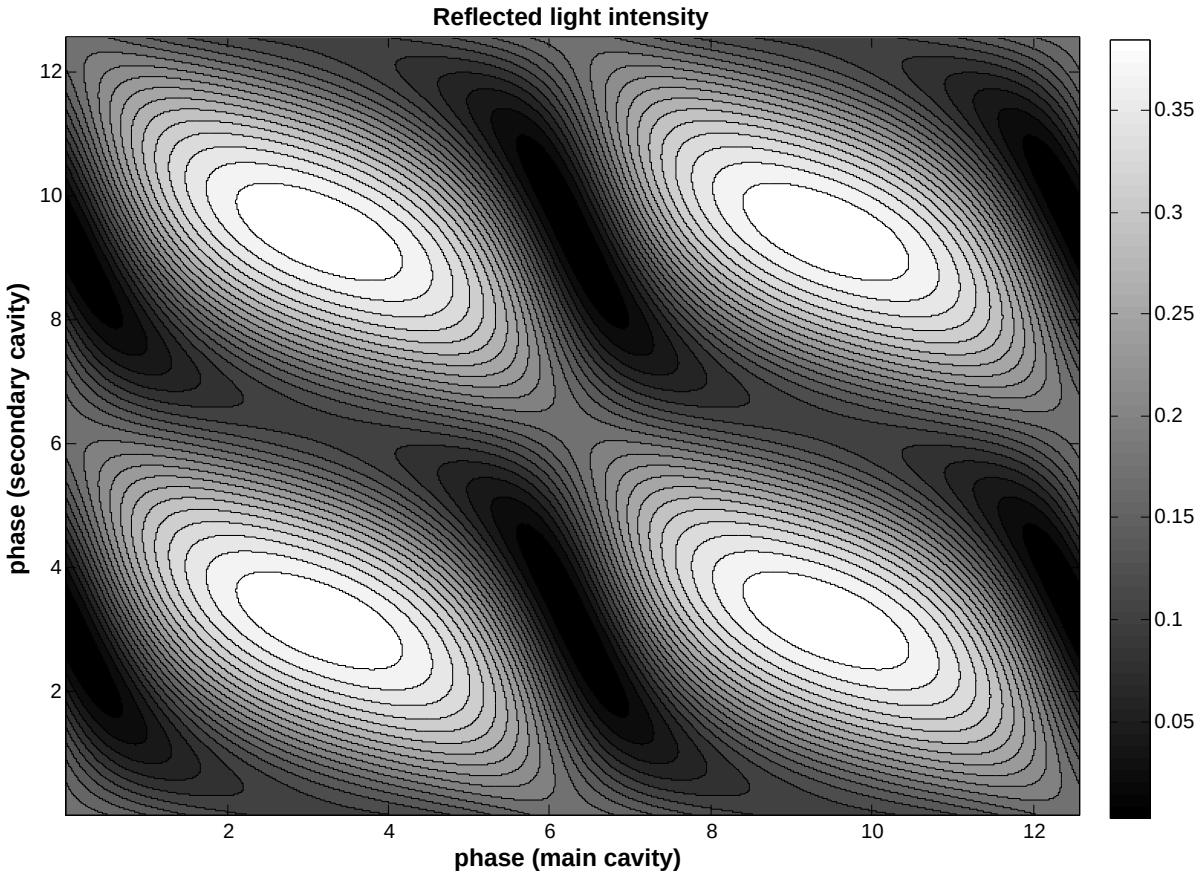

Figure 5.3: The reflection response of the compound cavity when coupling loss and main cavity loss are plugged in from the analysis in chapter 3.

The dependence on the round trip phase of the secondary cavity becomes stronger when absorption is considered in addition to loss. Figure 5.4 shows the result of plugging in the measured absorption at $794.6nm$ for a half round trip (optical depth of 2.29) from chapter 4, equation 5.3 .

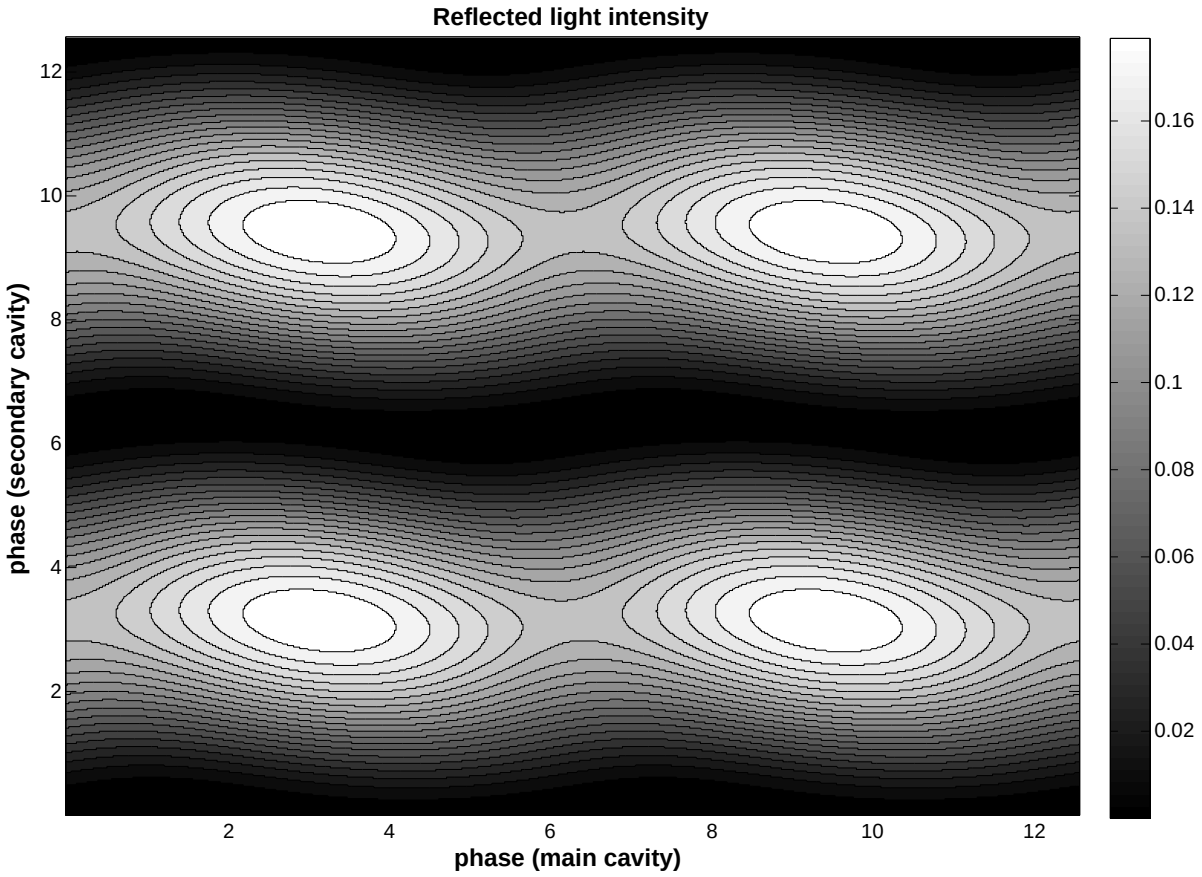

Figure 5.4: The reflection response of the compound cavity when coupling loss and main cavity's loss and absorption are plugged in from the analysis in chapter 3.

During the course of the experiment we changed the round trip phase of the secondary cavity by changing the distance between the fiber and the crystal surface. The round trip phase of the main cavity can be changed by adjusting the laser's frequency. The quantity that has been monitored is the efficiency. Although figure 5.4 depicts the reflected light intensity, as stated in the previous section, maximum absorption corresponds to maximum efficiency when the variables are round trip phases.

5.4 The impact of compound cavity on measurements of loss and absorption

The results of the previous section were based on measurements of loss and absorption in chapter 4 in which reflection from the fiber's front surface was ignored. If the fiber's front surface reflection is not neglected, the values of loss and absorption inside the main cavity and loss inside the secondary cavity (coupling loss) can be measured from equation 5.3 *if* the round trip phases of the main and secondary cavities are known. From one set of measurements of maximum and minimum reflection from the cavity, loss and absorption values can not be derived since there are four unknowns. However the effect of the cavity on the loss measurements can be estimated using appropriate approximations. Even though the discussion in section 5.2 shows that the maximum absorption does not happen exactly at the main cavity's resonance, figure 5.2 shows that maximum absorption happens *around* the main cavity's resonance. By putting the main cavity on resonance in equation 5.3 the values of loss (or absorption) in the main cavity and loss in the secondary cavity can be calculated numerically for each value of the secondary cavity's round trip phase. In the last chapter we indicated that we have three measurement sets at hand. One measurement set corresponds to the laser's frequency and polarization on resonance with atoms. Another measurement set is taken when the laser's frequency is resonant with the atoms but it's polarization is "off resonance". Finally, one measurement set is taken when the beam's polarization is "on resonance" with the the atoms but the frequency is off resonant with the atoms. The loss inside the secondary cavity, which in the language of the previous chapter is the coupling loss, should be almost the same for all three sets of measurements. This intuitive concept is reinforced by mathematical calculations in the last chapter, based on which the three measurement sets yield coupling loss to be between 58% to 60%.

By considering the aforementioned fact, the three sets of measurements make it possible to reckon the round trip phase of the secondary cavity, since the round trip phase must have a value that matches with the fact that coupling loss must stay constant. Numerical

calculations show that the round trip phase should be around 2 radians. With this value of the secondary cavity round trip phase, the numerically derived effective values of r_3 (r'_3, including loss and absorption) are 0.11, 0.18 and 0.68 in the case of the frequency and polarization on resonance with the atoms, the frequency on resonance with the atoms but polarization off resonance with the atoms, and neither frequency nor polarization on resonant with the atoms, respectively. The corresponding values that were derived in the previous chapter are 0.07, 0.17 and 0.69. Within the precision of the measurements, there is no significant difference between the values derived in this chapter and those derived in the previous chapter.

Chapter 6

THE EXPERIMENTAL RESULTS

6.1 Making an AFC inside a cavity, review of challenges

In the proposal of [23] the theoretical analysis is based on the assumption that a uniform AFC exists inside the cavity. However making an AFC inside the cavity is not a straight forward task. The complication stems from two separate facts.

First, the cavity disturbs the uniformity of the burning pulses (or beams) which as defined in chapter 2, are the pulses (or beams) that prepare the AFC by tailoring the absorption spectrum. Depending on the frequency interval between the cavity's resonance and the input frequency of the light, the intensity of the light can be magnified or reduced as mentioned in chapter 3, section 3.1 and depicted in figure 3.1. This point becomes more pronounced in a high finesse cavity which is a requirement for approaching 100% quantum memory efficiency.

Second, changing the absorption spectrum at any frequency alters the cavity response[1] at adjacent frequencies. For a crystal that is not enclosed by a cavity, the absorption spectrum at any frequency can be changed without affecting the response of the crystal to a monochromatic field at any other frequency. This is because the crystal responds to an input field as $E_o = e^{k_r + ik_i} E_i$ where k_r and k_i are the real and imaginary parts of the wave number. What is measured in the frequency domain is the absolute value squared of the electric field, which is not dependent on the dispersion spectrum. Consequently, although the Kramers-Kronig relations demand alteration of the dispersion spectrum at all frequencies when the absorption spectrum is changed (see chapter 2, section2.1), the crystal response remains uncorrelated at distinct frequencies. However, this is not the case if the crystal is enclosed in a cavity.

[1] For the definition of "response of a physical system" look at footnote 3 in page 11. Note that "response" is defined as an abstract concept and is independent of measurement. On contrast, measurement is dependent on response.

Equation 3.2 shows that the dispersion spectrum has a direct impact on the cavity response in the frequency domain. Therefore, changing the absorption spectrum at any frequency alters the cavity response at nearby frequencies. This makes it complicated to read out the AFC since the cavity response has to be known over a large range [2] of frequencies and then the Kramers-Kronig relations, together with the response function of the cavity (off resonant with the atoms in the frequency domain) must be used to derive the absorption spectrum of the crystal. The requirement of knowing the response at a large frequency interval and intricacies of the required algorithm, made us to look for an alternative method.

In [27] just four absorption peaks were created and the whole AFC was less than 4 MHz wide, while the cavity's linewith was roughly 300 times larger. So in practice the authors bypassed the complication of non uniform intensity of the burning pulses. The AFC was not read out in the experiment but the authors used an uncoated part of the crystal to measure the absorption spectrum when using the same burning sequence. However, as mentioned in the paper, the method just provided a rough guess for the AFC parameters. In an earlier paper by the same group [29], rough approximations, based on the slow light effect (see chapter 4 and appendix C) and assuming that $\tilde{d} \ll 1$ was used to provide a best guess on the AFC parameters.

In the experiment of reference [26] the cavity linewidth was comparable into the AFC width but the burning beams were sent into the crystal at a small angle with respect to the cavity axis, so the authors could avoid the complications of making the AFC within a cavity profile. The AFC parameters were put in calculations by considering the required value for $\tilde{d}$ for the impedance matching condition and assuming negligible intracavity loss, together with the known value of medium's optical depth (before making the AFC).

In our experiment, as stated in chapter 4, the burning pulses are sent into the cavity through its front surface. Since the cavity linewidth is around 10 GHz and the AFC width

[2] Large enough to make the impact of frequencies out of the range negligible on the dispersion spectrum at the considered point.

is 100 MHz, (as in [27] and [29]) we can ignore the effect of the cavity profile for the optical pumping. To estimate the AFC parameters, we use the cavity response in the time domain, together with the calculated value for absorption and loss in chapter 5.

6.2 Pulse train as a means of burning an AFC

As stated in chapter 2 section 2.1, the Fourier transform of the Shah function in the frequency (time) domain is another Shah function in the time (frequency) domain. This fact formed the base for the AFC concept as a frequency filter. It was mentioned that in a physical frequency filter, absorption peaks have a finite width, which, when transformed into the time domain packages (covers) the comb structure [3]. Likewise, a uniform pulse train is basically a comb in the time domain that when studied in the frequency domain forms a comb that is packaged by the Fourier transform of a single pulse.

To make an AFC in the experiment (the experimental setup is described in chapter 4) , in one measurement we sent 100 uniform pulses into the crystal, each 10 ns wide and with pulse separation 96 ns. Figure 6.1 shows the Fourier transform of the 100 Gaussian shaped pulses, assuming 96 ns interval between adjacent pulses.

[3] The absorption peaks are the narrowest features in the frequency domain. Therefore their Fourier transform is the widest feature in the time domain and "packages" the whole structure in the time domain.

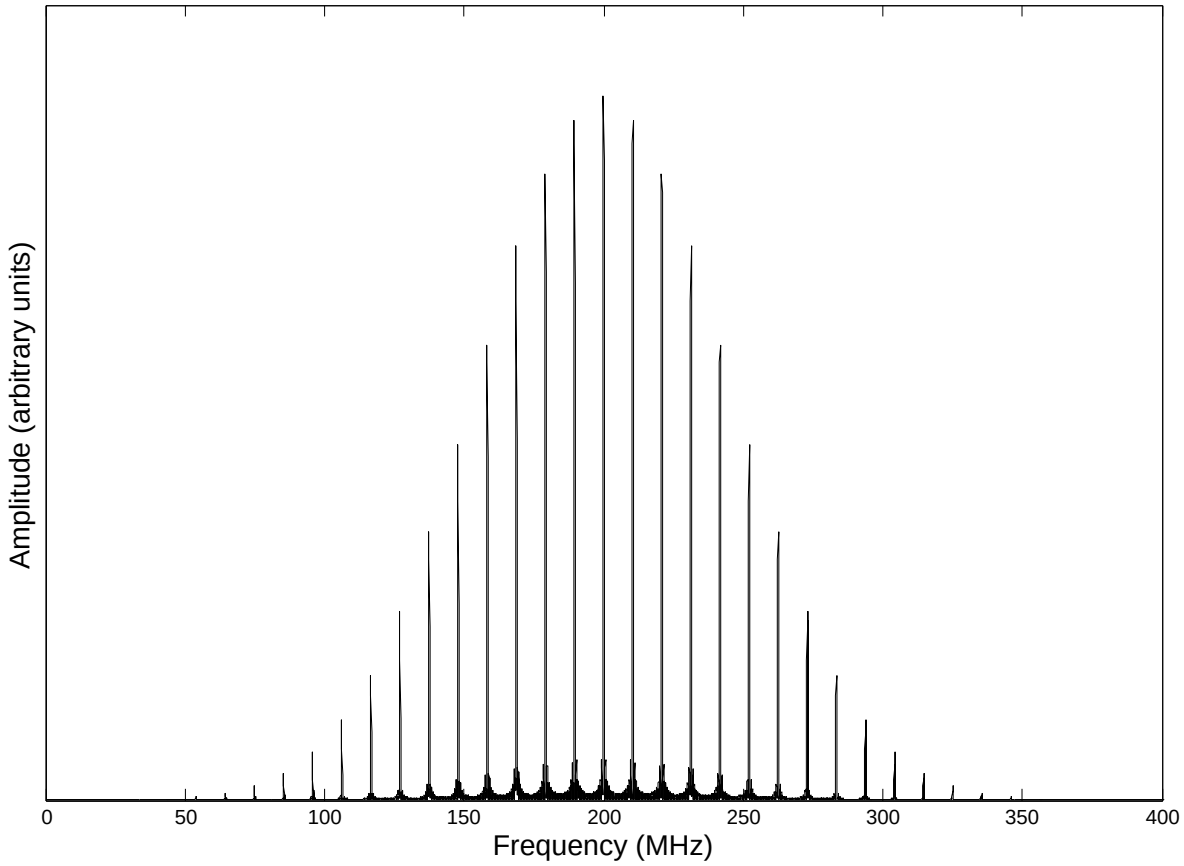

Figure 6.1: The (absolute value of) Fourier transform of a train of 100 pulses. Each pulse is 10 ns wide and the interval between them is 96 ns. Gaussian shape is assumed for the pulses. The reference frequency is arbitrary and the peaks somewhat deviate from the ideal Dirac delta shape due to the finite number of pulses in the time domain.

Figure 6.1 shows that sending the mentioned pulse train into the crystal would imprint an AFC pattern with low finesse (less than 2) in the absorption spectrum [4]. Figure 6.2 shows the experimental response of the cavity that included the memory crystal, to a pulse train with the aforementioned features.

[4] The AFC finesse is defined in chapter 2.

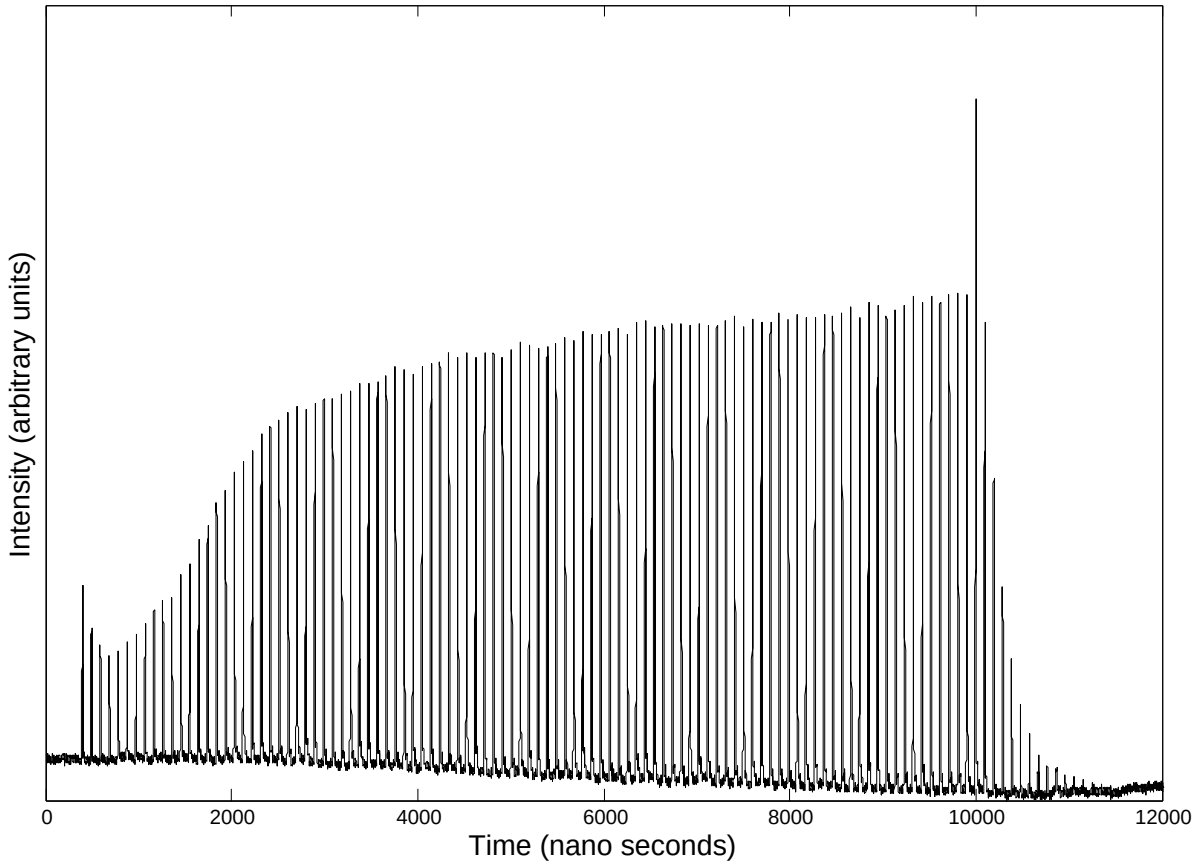

Figure 6.2: The intensity of pulses reflected off the cavity in the experiment. Each pulse was 10 ns wide and pulse separation was 96 ns. The measurement was done at 794.6 nm and the main cavity (refer to chapter 5) was close to resonant. The trace was averaged over individual measurements that were repeated every 5 ms.

The first few reflected pulses follow a diminishing power pattern. This is because the main cavity at first has a large value of loss plus absorption with optical depth 2.21 (look in chapter 5), which is beyond what corresponds to the impedance matching condition. The first pulses reduce the absorption in the medium and as the system gets closer to the impedance matching condition, the intensity of the reflected pulses reaches a minimum. The compound cavity, which is formed because of the fiber's front surface reflectivity, is responsible for the non-zero intensity at the impedance matching condition. As further pulses are sent in, the absorption inside the cavity continues to diminish and so the intensity of the reflected pulses

start to increase. After the 22nd (or so) pulse is send in, there remains almost no absorption in the medium and hence the reflected pulses have a higher intensity and are merely identical. Finally, after the reflection of the last pulse from the medium, echoes are seen. These are a combination of transient and persistent echoes (defined in chapter 2). The persistent AFC is formed since the measurement is repeated every 5 ms and the life time of persistent holes exceeds 5 minutes in our measurements.

Although the echoes in figure 6.2 are a combination of persistent and transient echoes, their Fourier transform provides an estimation of the AFC finesse. The Fourier transform is shown in figure 6.3.

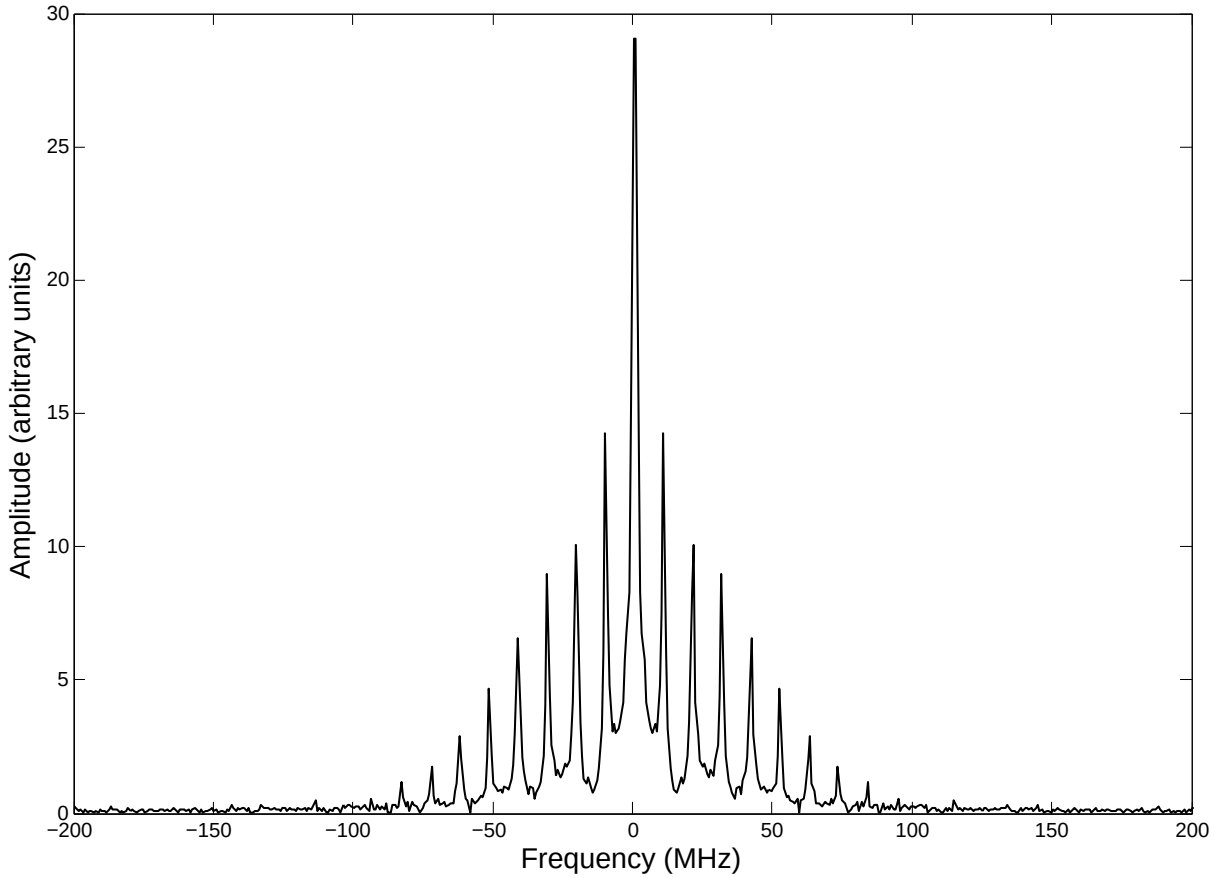

Figure 6.3: The echo pulses of figure 6.4 in the frequency domain (absolute value). The finesse of the related AFC is estimated as F=1.2 .

Following the discussion in chapter 3, the above figure shows the reflection profile of the

cavity that covers the AFC, multiplied by the input pulse in the frequency domain. However the individual peaks show the frequencies at which the light experiences minimum absorption by the atoms, due to the AFC structure. The AFC finesse is estimated to be F=1.2 .

Similarly, in another measurement we sent to the crystal 100 pulses, each 10 ns wide and separated by 25 ns. Figure 6.4 shows the cavity response to that pulse train.

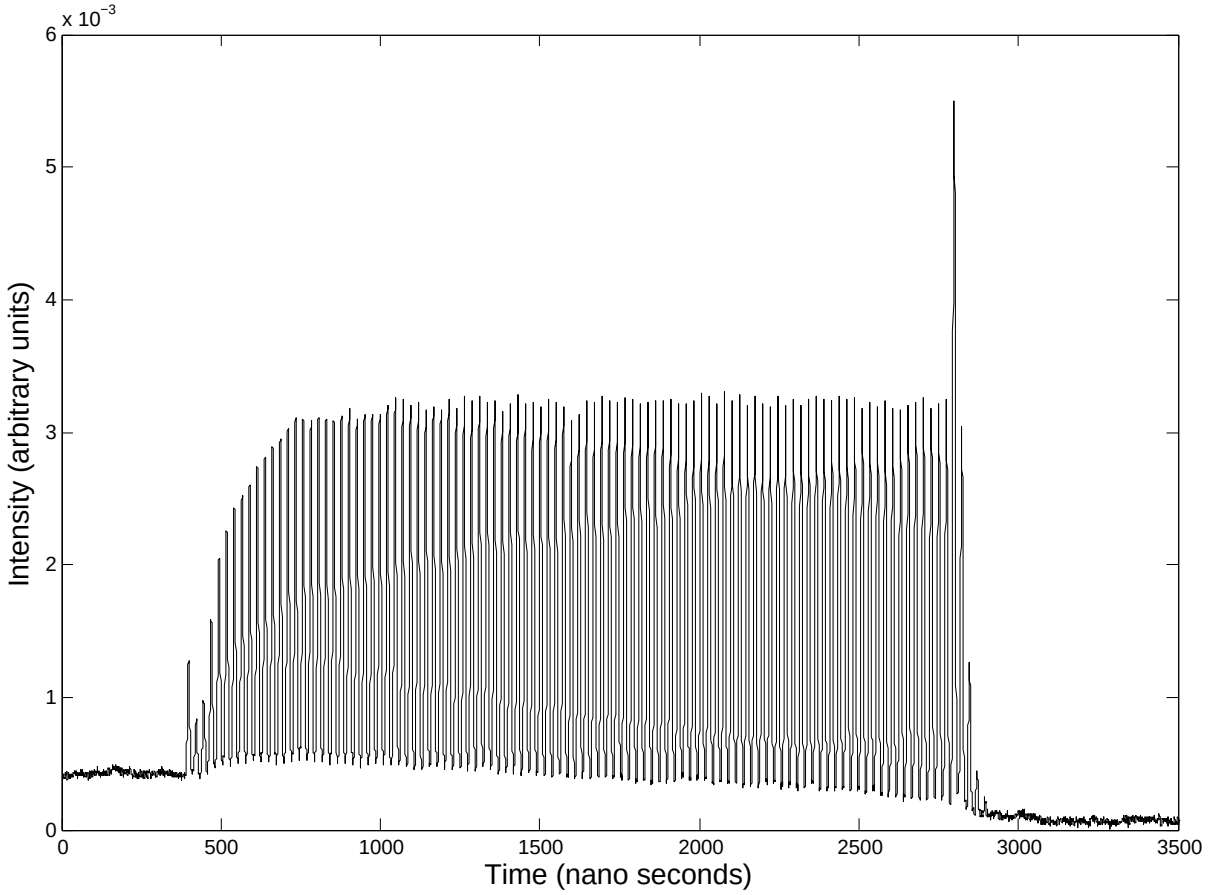

Figure 6.4: The power of pulses reflected off the front surface of the cavity in the experiment. Each pulse was 10 ns wide and pulse separation was 25 ns. The measurement was done at 794.6 nm and the main cavity (refer to chapter 5) was close to resonance. The trace was averaged over individual measurements that were repeated every 5 ms.

Figure 6.5 shows Fourier transform of the echo pulses of figure 6.4 to the frequency domain.

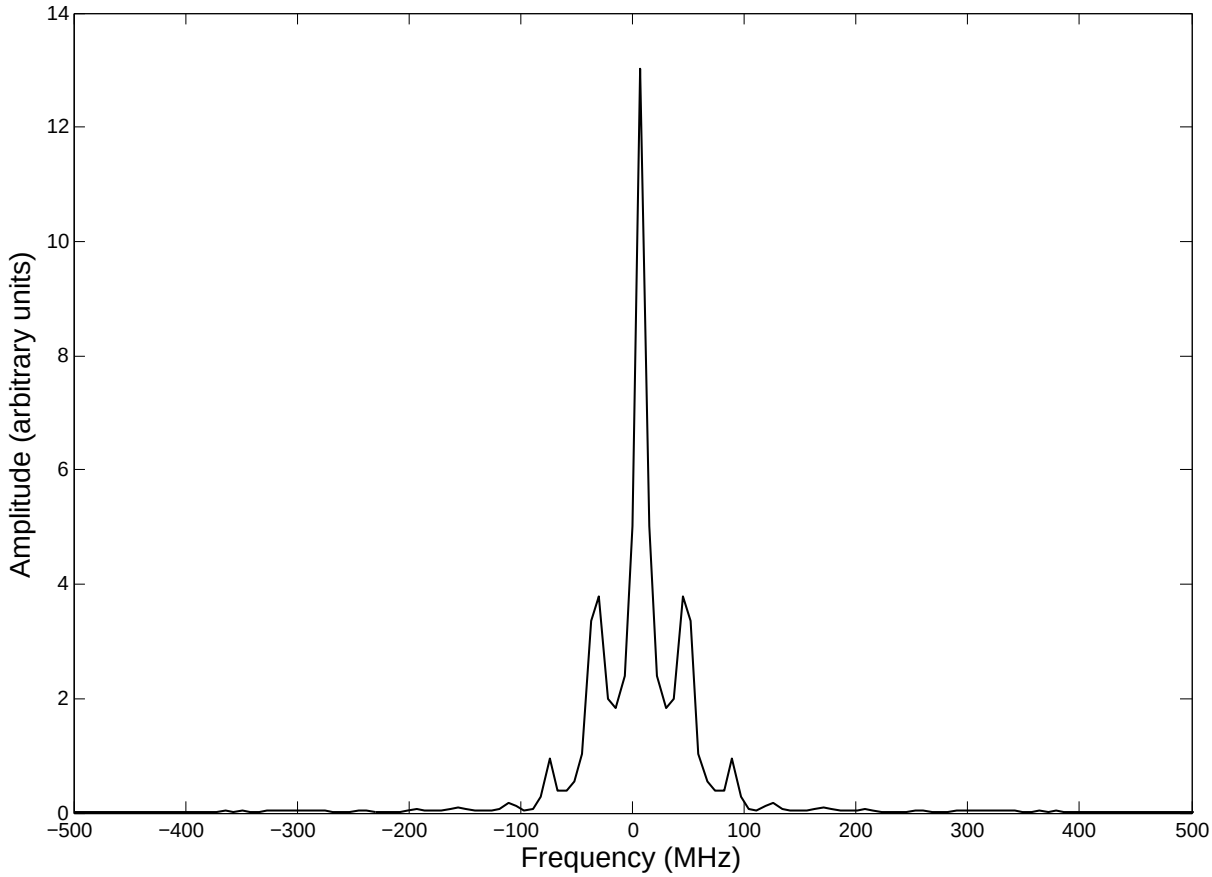

Figure 6.5: The echo pulses of figure 6.4 in the frequency domain (absolute value). The finesse of the related AFC is estimated as F$\simeq$1.6 .

6.3 Persistent AFC carved by a pulse train.

6.3.1 The experimental result

The cases studied in the last section are a combination of persistent and transient echoes. A transient AFC is not considered a quantum memory since spontaneous emission may amplify the echoes. For getting a purely persistent AFC and thus persistent echoes, a wait period has to be added before sending the probe pulse such that any transient AFC will decay. The wait time in the measurement presented in this section is 5 ms and, after sending the probe pulse, the experiment is repeated and the results are averaged over time. The highest efficiency in the experiment is achieved when the pulse separation in the pulse train is 25 ns.

The following figure shows the persistent echoes and reflected pulse from the cavity with the aforementioned conditions for the burning sequence.

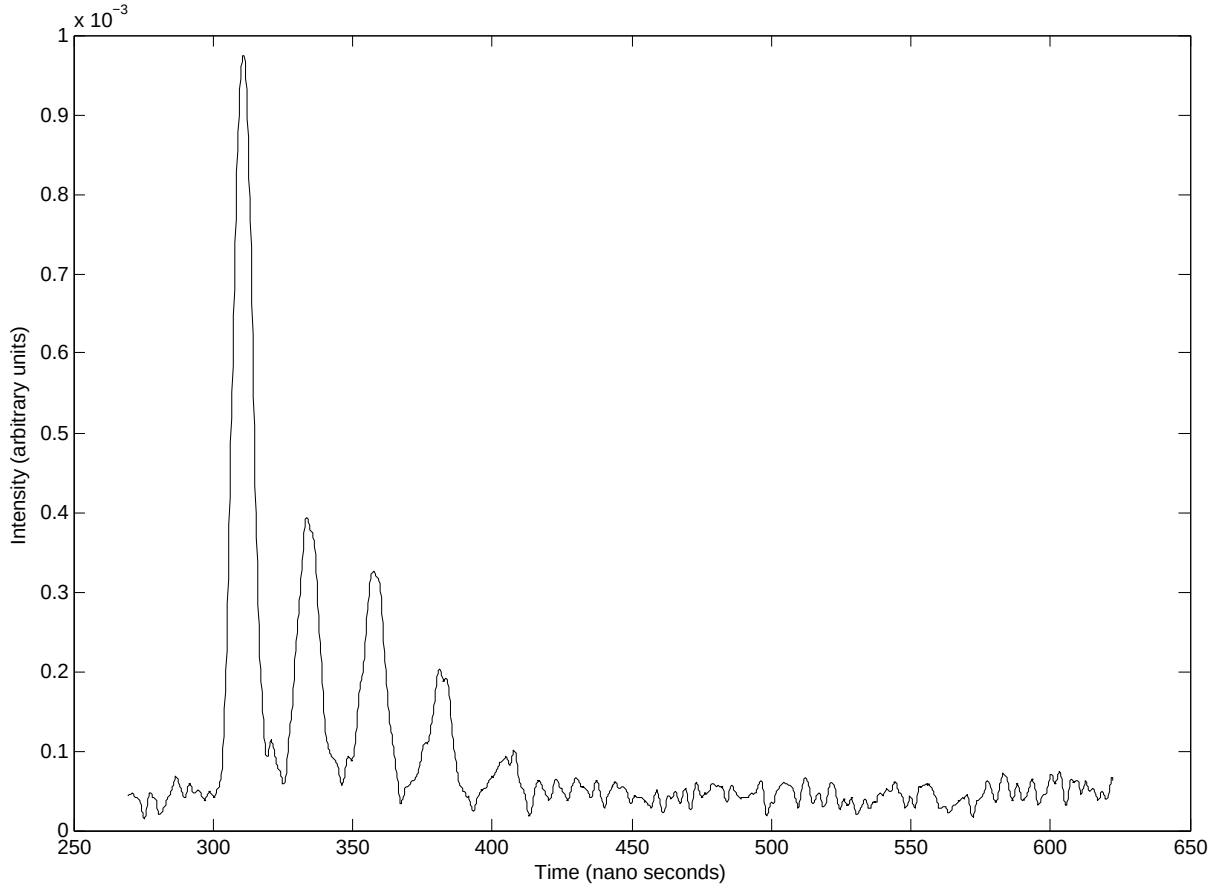

Figure 6.6: Intensity of the probe pulse reflected back of the cavity and persistent echoes after 5 ms wait, following the pulse train in figure 6.4.

The corresponding Fourier transform can be taken, but is not very clear since echoes are relatively weak and close to the background noise. However, figure 6.5 provides a reasonable guess of the AFC finesse. Even though it is taken from the combined response of transient and persistent AFCs there should not be a considerable difference between the finesse in the two cases. The Fourier transform of figure 6.6 also shows a clear resemblance with figure 6.5, in spite of the parts lost due to poor resolution and background noise. Therefore we use the value F=1.6 in the efficiency analysis subsections.

6.3.2 Efficiency analysis, the simple cavity approach

A cavity enhanced AFC with a finesse F=1.6, a value of loss $d_0 = 0.36$, coupling coefficient to the fiber $\alpha = 0.59$, front mirror reflectivity $R_f = 0.14$ and back mirror reflectivity $R_f = 1$ results in an efficiency as a function of optical depth as shown in figure 6.7. The figure also shows the efficiency of an identical memory that is not cavity enhanced (a bare crystal). Relations 3.8 and 2.8 are employed to derive the figure.

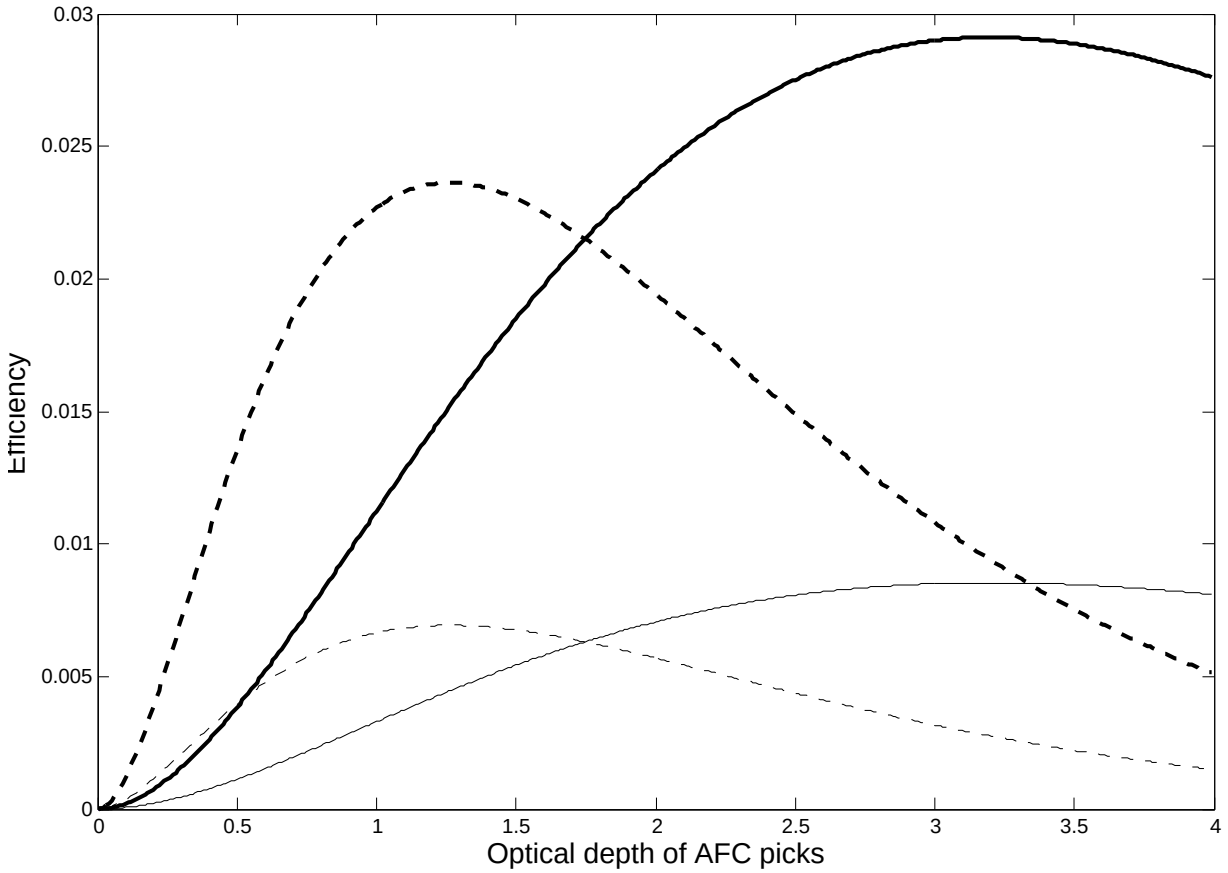

Figure 6.7: Theoretical efficiencies of an AFC. a) Solid thick line: Square shaped bare AFC b) Dashed thick line: cavity enhanced square shaped AFC. c) Solid thin line: Gaussian shaped bare AFC d) Dashed thin line: Cavity enhanced Gaussian shaped AFC. The loss, optical depth (in half round trip), the coupling from waveguide to the fiber, finesse, and the front mirror reflectivity are set to $d_0 = 0.36$, $\alpha = 0.59$, $F = 1.6$, and $R_f = 0.14$, respectively.

The power of the first echo in figure 6.6 is measured to be 2% of the input beam power by scaling to the pulse that bounces off the fiber surface when the fiber was above the crystal. Figure 6.7 shows that the measured efficiency is close to the maximum value achievable theoretically for the employed waveguide. The value of d_1 in chapter 5 is given to be around 1.8. Nevertheless this value may have reduced after making the AFC. The impact on the efficiency however is probably too small to be detected in the experiment.

6.3.3 Efficiency analysis, the compound cavity approach

Using equation 5.6 helps to derive the effect of the fiber's surface reflectivity on the compound cavity's efficiency. By plugging in the numbers mentioned above for coupling, loss, absorption, finesse and corresponding mirror reflectivities the following figure gives the efficiency as a function of round trip phases of main and secondary cavity.

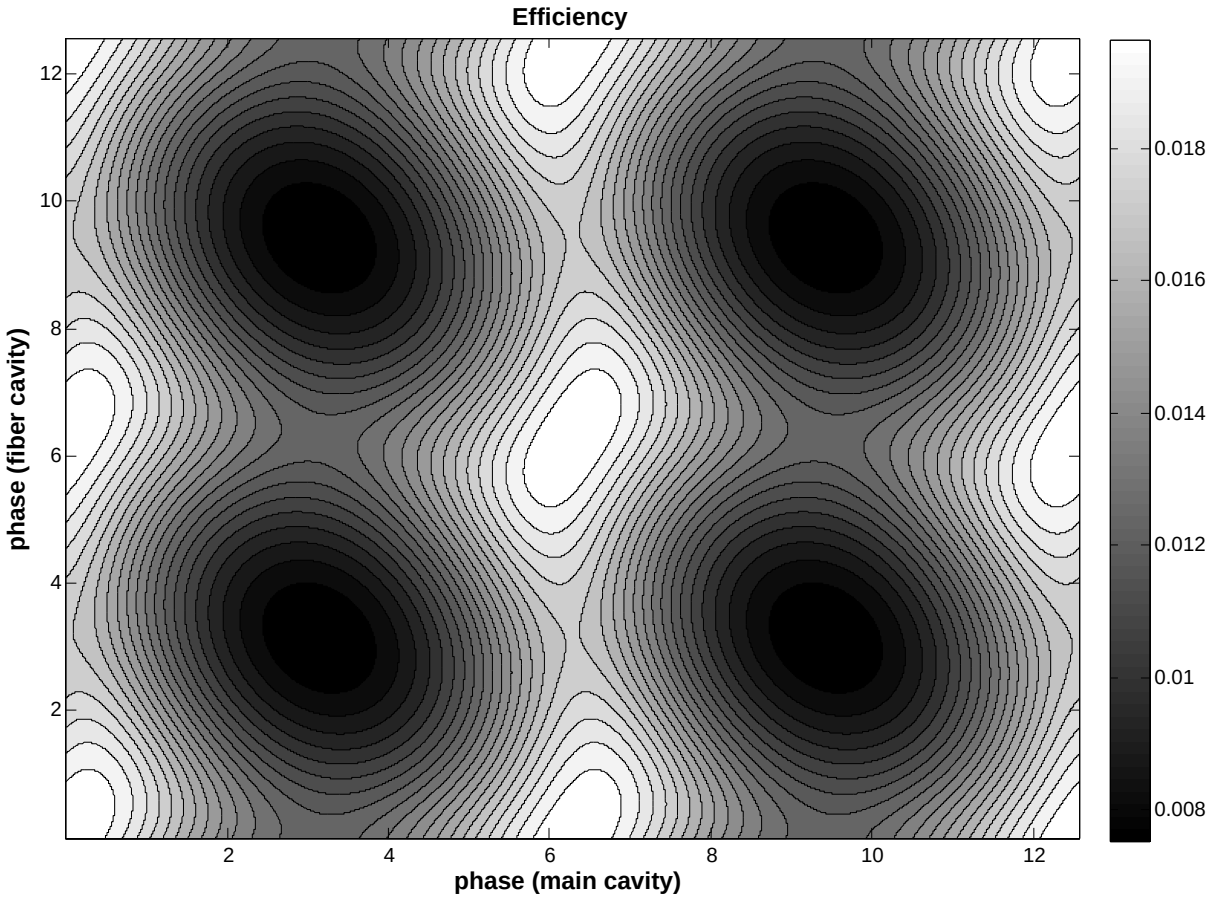

Figure 6.8: Theoretical efficiency of a square shaped AFC when put in a compound cavity with mirror reflectivities $R_1 = 0.04$, $R_2 = 0.14$ and $R_3 = 1$. The loss optical depth (in half round trip), coupling from waveguide to the fiber, absorption optical depth and finesse are $\alpha = 0.59$, $d_0 = 0.36$, $d_1 = 1.82$ and $F = 1.6$ respectively.

By considering the round trip phase of the main and secondary cavity estimated in the previous chapter (0 and 2 radians, respectively), figure 6.8 shows that the efficiency was around 90% of the maximum theoretical value.

Chapter 7

SUMMARY AND OUTLOOK

Even though the unanticipated high loss inside the main cavity rendered our efforts to create a high efficiency quantum memory fruitless, the experiment and the subsequent analysis provide valuable knowledge and insight into the dynamics of a cavity-enhanced AFC memory and the structure of waveguides that -in principle- can provide a more convenient and integrated way to implement an AFC based quantum memory than the use of a bulk crystal. We can summarize the achievements and their possible application in the future in three points:

1. The experiment manages to identify the obstacles to get high efficiency for a waveguide quantum memory. It provides a direct measurement of the intracavity loss and coupling loss from the fiber to the waveguides. In reference [28] the overall fiber-to-fiber loss was reported to be 15 dB for a 15.7 mm waveguide crystal . The measurement of coupling (fiber to waveguide *or* waveguide to fiber) and the optical depth of intracavity loss (for half a round trip) in chapter 4 are 0.59 and 0.36, respectively, for a 2 mm long waveguide crystal. For a hypothetical 15.7 mm crystal, coupling should not change but the optical depth of the intracavity loss would increase to 2.81. These values yield an overall fiber-to-fiber loss of 16.8 dB, which is close to the value reported in [28]. Nevertheless, in [28] (as well as [1]) the whole fiber-to-fiber loss was attributed to coupling loss. The analysis in chapter 4 (as well as chapter 5) suggests that intra-waveguide loss (probably due to scattering), has a much bigger impact than coupling loss.

   The source of this intra-waveguide loss, however, remains unknown. In [30] the

maximum value for the intra-waveguide loss was reported to be 0.46 dB/cm. The measured value in our experiment is 7.81 dB/cm. Damaged waveguide surfaces due to handling and defects of the cavity surface [31] are among the possible reasons responsible for the large amount of intra-waveguide loss. Whatever the reason, it has to be carefully investigated before proceeding on any future implementation of a cavity-enhanced waveguide AFC quantum memory, because it basically prevents the efficiency from improving as a result of employing a cavity.

2. Investigation of the optimal conditions for a cavity-enhanced AFC, when the quantity that can be changed is the optical depth. This clarified a generally overlooked fact that impedance matching does not necessarily coincide with the optimized condition for AFC efficiency. Ignoring this fact can result in misinterpretation of results and inadequate experimental settings being used.

3. The study of a compound cavity-enhanced AFC in chapter 5, which was mainly motivated by the observations during the alignment of the fiber to the waveguide, can potentially be used for finding the impedance matching condition. It can also be employed for creating the AFC and reading it out inside the cavity without facing the intricacies due to the cavity response. Adjusting the resonance of the compound cavity in the frequency domain is another potential application of a compound cavity-enhanced AFC that can remove concerns of having the resonance off the AFC due to the slow light effect (see references [27] and [29]).

Appendix A

The code for computing efficiency of an AFC

```
1  %This MATLAB code computes the efficiency of a plian AFC as a function of
       optical depth
2  % @Hassan Mallahzadeh, Oct 2014
3  set(0,'DefaultFigureWindowStyle','docked')
4  close all
5  clc
6  %Note: The unit of frequency is MHz and the time unit is microsecond
7
8  %The background index of refraction
9  nr=2;
10 %The atomic medium length (in meters)
11 LL=0.002;
12 %The time resolution
13 step=0.1;
14 %The time limit. Note: Resolution of the frequency domain is the
15 %inverse of the time range
16 tlimit=10000;
17 tt=-tlimit:step:tlimit;
18 %Prepares the frequency domain
19 vv=fftshift(fftconj(tt));
20 %Sorts the vv array
21 vv=sort(vv);
22 %Finds and stores size of the frequency and the time arrays in "S" and
23 %"ST" variables
24 [D,S]=size (vv);
25 [DT,ST]=size(tt);
26 %The input Gaussian pulse in the time domain
```

```
27 sigma=1;
28 Pulse=(exp(-(tt).^2/sigma^2));
29 %The pulse in the frequency domain is derived here
30 PulseF=fftshift(fft(ifftshift(Pulse)));
31 %Pick to pick seperation (AFC)
32 dv=0.5;
33 %Finesse(AFC)
34 F=2;
35 %Finds the maximum and minimum of the frequency array and their corresponding
36 %locations in the array
37 [MinVV nMin]=min(vv);
38 [MaxVV nMax]=max(vv);
39 %Finds the limits of AFC in the frequency array
40 Kup=fix(MaxVV/dv);
41 Kbot=fix(MinVV/dv);
42 %Gaussian AFC
43 GAFC=zeros(size (vv));
44 a=dv/(F*2*sqrt(log(2)));
45 for k=Kbot:Kup
46 GAFC= GAFC+exp(-(vv-k*dv).*(vv-k*dv)/(a*a));end
47 %Lorentzian AFC
48 LAFC=zeros(size (vv));
49 etta=dv/(2*F);
50 for k=Kbot:Kup, LAFC=LAFC+etta./((vv-k*dv).*(vv-k*dv)+etta*etta);end
51 LAFC=LAFC*etta;
52 %Square AFC
53 SAFC=zeros(size(vv));
54 FW=0.5-(1/F);
55       dvS=dv/2;
56       j=fix(MinVV/dvS);
57 while(dvS*j<MaxVV)
58       if(rem(j,2)==0)
```

```
59      SAFC=SAFC+tanh(10000*(vv-dvS*j+(1/(F))*dvS))*(-1)^(j+1);
60        else
61      SAFC=SAFC+tanh(10000*(vv-dvS*j+FW*dv+(1/(F))*dvS))*(-1)^(j+1);
62        end
63        j=j+1;
64  end
65  %Setting the minimum optical depth equal to zero
66  MinOD=find(vv>=(dv/2));
67  GAFC=GAFC-GAFC(MinOD(1));
68  LAFC=LAFC-LAFC(MinOD(1));
69  SAFC=SAFC-SAFC(MinOD(1));
70  %Scales the AFC peaks' optical depth equal to one
71  ZFreq=find (vv>=0);
72  GAFC=GAFC./GAFC(ZFreq(1));
73  LAFC=LAFC./LAFC(ZFreq(1));
74  SAFC=SAFC./SAFC(ZFreq(1));
75  % Calculates the actual finesse of the Gaussian AFC
76  for i=1:floor(S/2)
77  if GAFC(ZFreq(1)+i-1)<=0.5
78  Gfinesse=dv/(vv(ZFreq(1)+i-1)*2);break,end
79  end
80  % Calculates the actual finesse of the Lorentzian AFC
81  for i=1:floor(S/2)
82        if LAFC(ZFreq(1)+i-1)<=0.5
83                  Lfinesse=dv/(vv(ZFreq(1)+i-1)*2);break,end
84  end
85  % Calculates the actual finesse of the square AFC
86  for i=1:floor(S/2)
87        if SAFC(ZFreq(1)+i-1)<=0.5
88                  Sfinesse=dv/(vv(ZFreq(1)+i-1)*2);break,end
89  end
```

```
90  % The pit (transparent window) inside the absorption spectrum that contains
        the AFC
91  Pit=(-tanh(10000*(vv-(fix(mean(vv))-1)))+tanh(10000*(vv-(fix(mean(vv))+1))))
        *0.5;
92  % Settinging the minimum of optical depth of the pit to be equal to zero
93  MinOD=find((vv>=0));
94  Pit=Pit-Pit(MinOD(1));
95  % Removes the AFC structure outside the pit
96  Imag=((1-Pit).*SAFC*(1)+(Pit));
97  % Finds the dispersion spectrum
98  Real=imag((conv(1./(1i*vv),Imag,'same')*(vv(2)-vv(1)))/(pi));
99  % The "root" AFC exponent, to be modified by the desired optical depth
100 AFCRoot=(1i*Real+Imag);
101 % Maximum obtainable optical depth
102 d1Max=10;
103 % The step size that the optical depth changes in the code
104 step=0.1;
105 % Number of steps
106 d1Steps=fix(d1Max/step);
107 % The array that stores amplitudes of first echoes
108 PowerArray=zeros(d1Steps);
109 d1=zeros(d1Steps);
110 for i=1:d1Steps
111 d1(i)=step*(i-1);
112 %loss
113 d0=0;
114 % Setting the peaks' optical depth
115 AFC=(AFCRoot*d1(i)+d0)/2;
116 % In this part the response in the frequency domain is calculated.
117 KAPPA=(1i*vv*(nr/3)*0.01*LL+AFC);
118 Profile=exp(-KAPPA);
119 TransF=PulseF.*Profile;
```

```
% Fourier transformation to find the response in the time domain
TransT=real(fftshift(ifft(ifftshift(TransF))));
% This part finds the intensity of the first echo
power=0;
k=1;
% This loop gives the freedom to consider other echoes
while k<2
echo=k*1/dv;
GT1=find(tt>=echo);
power=power+(TransT(GT1(1))).^2;
k=k+1;
end
% Finding the intensity of the light that is directly transmitted
GT2=find(tt>=0+zpt);
Tpower=(TransT(GT2(1))).^2;
PowerArray(i)=power;
end

%Figures
figure (1)
plot(tt, abs(Pulse).^2)
xlabel('time (micros)','FontSize',12,'FontWeight','bold')
ylabel('~absolute value','FontSize',12,'FontWeight','bold')
title(sprintf('pulse in time domain'),'FontSize',12,'FontWeight','bold')
xlim([-100 +100])

figure (2)
plot(vv, abs(PulseF).^2)
xlabel('Frequency (MHZ)','FontSize',12,'FontWeight','bold')
ylabel('~absolute value','FontSize',12,'FontWeight','bold')
title(sprintf('pulse in frequency domain'),'FontSize',12,'FontWeight','bold')

```

```
figure (3)
plot(vv,real(AFC))
xlabel('Frequency (MHZ)','FontSize',12,'FontWeight','bold')
ylabel('~Optical depth','FontSize',12,'FontWeight','bold')
title(sprintf('Dispertion spectrum of the root AFC'),'FontSize',12,'FontWeight','bold')

figure(4)
plot(vv,imag(AFC))
xlabel('Frequency (MHZ)','FontSize',12,'FontWeight','bold')
ylabel('~Optical depth','FontSize',12,'FontWeight','bold')
title(sprintf('Absorption spectrum of the root AFC'),'FontSize',12,'FontWeight','bold')

figure (5)
plot(d1,PowerArray)
xlabel('Optical depth','FontSize',12,'FontWeight','bold')
ylabel('Efficiency','FontSize',12,'FontWeight','bold')
title(sprintf('Efficiency as a function of optical depth'),'FontSize',12,'FontWeight','bold')
```

Appendix B

The intracavity field

The field inside a cavity can be calculated using the sum over all round trip approach. The cavity intrafield is what one deals with when making an AFC by sending burning pulses through the mirrors and this field interacts with atoms. In the following figure a sample cavity is considered with front mirror reflection amplitude of r_1 and back mirror reflection amplitude of r_2. E_0, E_r, E_t, E_+ and E_- are the input, reflected, transmitted, right and left traveling wave amplitude, respectively.

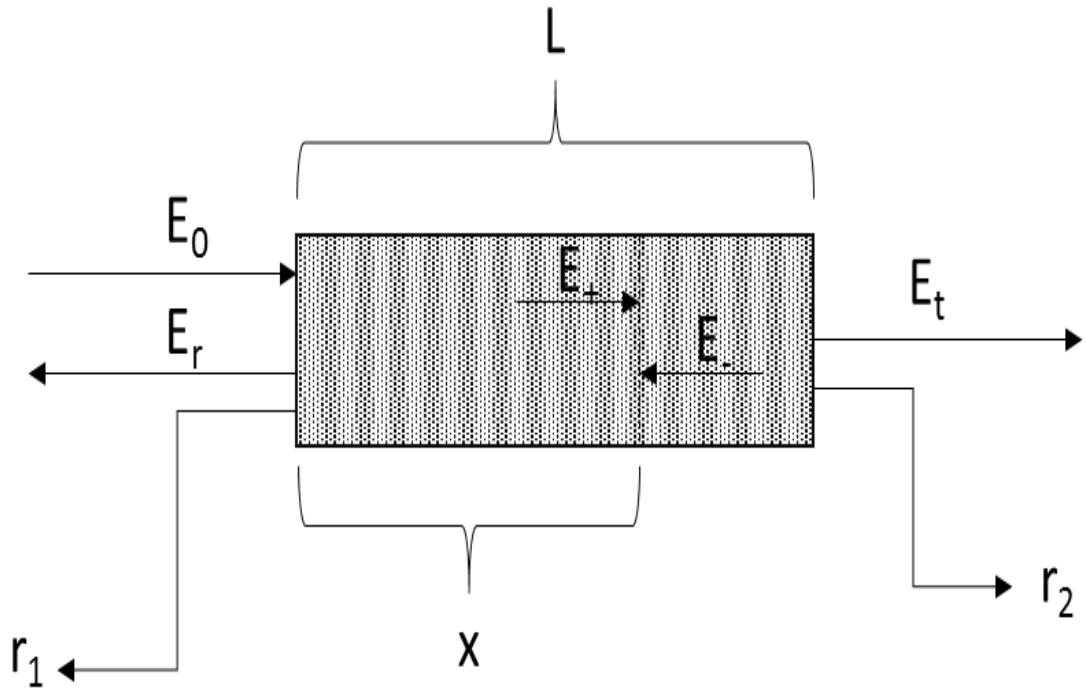

Figure B.1: A sample cavity with related variables to calculate the intracavity field (refer to the text).

The electric field at an arbitrary point x is given by the superposition of left and right traveling fields, which, considering the series of reflections from the mirrors and the stokes

relations ($r = -r^{'}$ and $r^2 + tt^{'} = 1$) are

$$E_+ = E_0 t_1 e^{ikx} \sum_{i=0}^{\infty} \left(r_1 r_2 e^{2ikL}\right)^i \ , \tag{B.1}$$

and

$$E_- = E_0 t_1 e^{ikx} r_2 e^{2ik(L-x)} \sum_{i=0}^{\infty} \left(r_1 r_2 e^{2ikL}\right)^i \ , \tag{B.2}$$

where k is the wavenumber, which might be complex. The absolute value of individual terms inside the summation are less than one. Therefore, using the identity $\sum_{i=0}^{\infty} (x)^i = \frac{1}{1-x}$ and the superposition principle, the total field at an arbitrary point x is

$$E_- + E_+ = E_0 t_1 e^{ikx} \left(\frac{1 + r_2 e^{2ik(L-x)}}{1 - r_1 r_2 e^{2ikL}}\right) \ . \tag{B.3}$$

Appendix C

The slow light effect

In a dispersive medium, the overall envelope of a pulse propagates with a group velocity that is given by [11]

$$V_g = \frac{d\omega}{dk_r} \ , \tag{C.1}$$

where ω is the angular frequency and k_r is the real part of the complex wavenumber which is denoted as $\tilde{k}$. The group index of refraction is defined by

$$n_g = \frac{c}{V_g} = c\frac{dk_r}{d\omega} \ , \tag{C.2}$$

in which c is the speed of light in vacuum. A square transparent spectral window (pit) inside an otherwise constant absorption spectrum can be defined by using the imaginary part of the wavenumber as

$$k_i(\omega) = \begin{cases} k_i = b & \text{if } |\omega| > \dfrac{w}{2} \ , \\ k_i = \dfrac{b}{2} & \text{if } |\omega| = \dfrac{w}{2} \ , \\ k_i = 0 & \text{if } |\omega| < \dfrac{w}{2} \ . \end{cases} \tag{C.3}$$

In the above, w is the width of the window, and $b = \dfrac{d}{2l}$ where d and l denote the optical depth and the crystal length, respectively. As stated in chapter 2, if k_0 (the background wavenumber) is subtracted from $\tilde{k}$ (the complex wavenumber), what remains ($\tilde{k} - k_0$) satisfies the Kramers-Kronig relations. Therefore, when k_i (the imagenary part of the wavenumber) is given, k_r (the real part of the wavenumber) may be derived by

$$k_r(\omega) - k_0(\omega) = \int_{-\infty}^{+\infty} \frac{k_i(\omega)}{\omega' - \omega} d\omega' \ , \tag{C.4}$$

in which $k_0(\omega)$ is given by $k_0(\omega) = \dfrac{\omega c}{n_0}$. Plugging C.3 into C.4 delivers

$$k_r(\omega) = k_0(\omega) + \frac{b}{\pi} \ln \left| \frac{\omega + w}{\omega - w} \right| \ . \tag{C.5}$$

Therefore, the group index of refraction can be calculated from C.2 and C.5 as

$$n_g(\omega) = \frac{2bc}{\pi} \left(\frac{w}{w^2 - \omega^2} \right) + n_0 \ , \tag{C.6}$$

and plugging C.7 into C.1 gives the group velocity as

$$V_g(\omega) = \frac{c}{\frac{2bc}{\pi} \left(\frac{w}{w^2 - \omega^2} \right) + n_0} \ . \tag{C.7}$$

As a check for validity, when ω approaches infinity (i.e. far from the window), $n_g(\omega)$ and $V_g(\omega)$ converge to n_0 and $\frac{c}{n_0}$. The latter are the values that one expects to get for the background. They also match with numerically calculated results in MATLAB.

At the center of the hole ($\omega = 0$), the group velocity from C.7 is

$$V_g(0) = \frac{c}{\frac{dc}{\pi^2 l \Gamma} + n_0} \ . \tag{C.8}$$

Figure C.1 shows how the group velocity changes as a function of optical depth, at the center of a $1GHz$ wide transparent window.

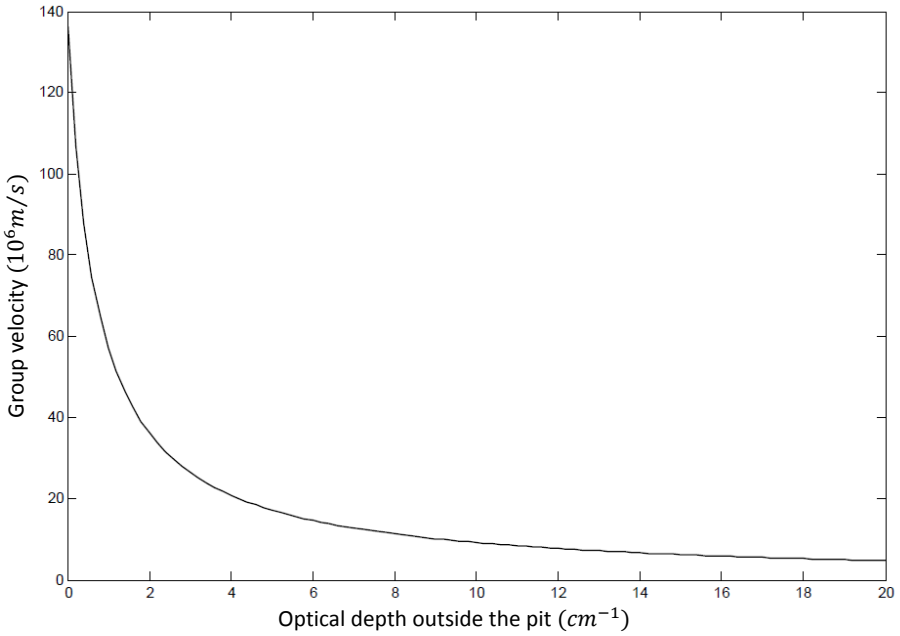

Figure C.1: Group velocity as a function of the optical depth per centimeter. The figure is associated with the group velocity at the center of a $1GHz$ wide square shaped transparent window. The curve is derived using equation C.7 by assuming the background index of refraction to be $n_0 = 2.2$.

Figure C.1 may be used for estimating the optical depth of an absorptive medium inside a cavity when the cavity response in the frequency domain is known. This is because the FSR if given by $\frac{V_g}{2L}$ [29]. Therefore, reduction of the FSR from what is calculated by putting the group velocity equal to the phase velocity, gives an estimation of the group velocity. For example, in the situation that is depicted in figure 4.4, the cavity FSR would have been seven times bigger if the measurement had been done without making a transparent window first. In figure C.1, the optical depth of zero corresponds to the case that no transparent window is made inside the absorption spectrum and the group velocity reduces by a factor of seven if the optical depth is around four per centimeter. Therefore, the optical depth of the medium in the measurement that corresponds to figure 4.4, must have been around four per centimeter.

Bibliography

[1] E. Saglamyurek et al. Broadband waveguide quantum memory for entangled photons. *Nature*, 469:512515, 2011.

[2] S. R. Hastings-Simonet et al. Zeeman-level lifetimes in er^{3+} : y_2sio_5. *Phys. Rev. B*, 78:085410, 2008.

[3] J. Preskill. Lecture notes for quantum information and computation. `http://www.theory.caltech.edu/people/preskill/ph229/`, 1998.

[4] A. I. Lvovsky et al. Optical quantum memory. *Nature Photonics*, (3):706 – 714, 2009.

[5] H. et al. Briegel. Quantum repeaters: The role of imperfect local operations in quantum communication. *Phys. Rev. Lett.*, 81, 1998.

[6] M. A. Nielsen and I. L. Chuang. *Quantum Computation and Quanum Information*. Cambridge U.P., 2000.

[7] N. Sinclair et al. Spectral multiplexing for scalable quantum photonics using an atomic frequency comb quantum memory and feed-forward control. *Phys. Rev. Lett.*, 113, 2014.

[8] M. Afzelius et al. Multimode quantum memory based on atomic frequency combs. *Phys. Rev. A*, 79:052329, 2009.

[9] M. Mitsunaga et al. Spectrally programmed stimulated photon echo. *Optics Letters*, 16(4):264–266, 1991.

[10] A.G. Marshall. *Fourier Transforms in NMR, Optical, and Mass Spectrometry*. Elsevier, 1989.

[11] D. Stek. Lecture notes for classical and modern optics. `http://atomoptics.uoregon.edu/~dsteck/teaching/optics`, 2013.

[12] M. Bonarota et al. Efficiency optimization for atomic frequency comb storage. *Phys. Rev. A*, 81:033803, 2010.

[13] N. Sinclair. Broadband quantum interface using a thulium-doped waveguide. Master's thesis, University of Calgary, Canada, 2010.

[14] M. Sabooni. *Efficient Quantum Memories Based on Spectral Engineering of Rare-Earth-Ion-Doped Solids*. PhD thesis, Lund University, Sweden, 2013.

[15] Nomenclature of inorganic chemistry: Iupac recommendations. `http://web.archive.org/web/20080527204340/http://www.iupac.org/publications/books/rbook/Red_Book_2005.pdf`, 2005.

[16] D. Johnson and P. Butcher. The lanthanides and actinides. `http://students.open.ac.uk/omresources/periodictable/ellaac/core.pdf`, 2006.

[17] D. H. Cornell. Rare earths from supernova to superconductor. *Pure and Appl. Chem.*, 65(12):2453–2464, 1993.

[18] E. Saglamyurek. *Broadband Waveguide Quantum Memory for Quantum Communication*. PhD thesis, University of Calgary, Canada, 2013.

[19] C. W. Thiel et al. Optical decoherence and persistent spectral hole burning in tm3+:linbo3. *Journal of Luminescence*, 130(9):1598 – 1602, 2010.

[20] N. Sangouard et al. Analysis of a quantum memory for photons based on controlled reversible inhomogeneous broadening. *Phys. Rev. A*, 75:039904, 2007.

[21] Q. Y. He et al. Dynamical oscillator-cavity model for quantum memories. *Phys. Rev. A*, 79:022310, 2009.

[22] F. Nilsson. Numerical simulations of atomic frequency comb quantum memories for long term storage. Master's thesis, Lund University, Sweden, 2012.

[23] M. Afzelius and C. Simon. Impedance-matched cavity quantum memory. *Phys. Rev. A*, 82:022310, 2010.

[24] J.E. Heebner et al. Optical transmission characteristics of fiber ring resonators. *Quantum Electronics, IEEE Journal of*, 40(6):726–730, 2004.

[25] S. A. Moiseev et al. Efficient multimode quantum memory based on photon echo in an optimal qed cavity. *Phys. Rev. A*, 82:022311, 2010.

[26] P. Jobez et al. Cavity-enhanced storage in an optical spin-wave memory. *New Journal of Physics*, 16:083005, 2014.

[27] M. Sabooni et al. Efficient quantum memory using a weakly absorbing sample. *Phys. Rev. Lett.*, 110:133604, 2013.

[28] N. Sinclair et al. Spectroscopic investigations of a $ti : tm : linbo_3$ waveguide for photon-echo quantum memory. *Journal of Luminescence*, 130:15861593, 2010.

[29] M. Sabooni et al. Cavity-enhanced storagepreparing for high-efficiency quantum memories. *New Journal of Physics*, 15:035025, 2013.

[30] R. Regener and W. Sohler. Loss in low-finesse ti:linbo3 optical waveguide resonators. *Applied Physics B*, 36(3):143–147, 1985.

[31] G. J. Sloggett. Fringe broadening in fabry-perot interferometers. *Appl. Opt.*, 23(14):2427–2432, 1984.